Available online at www.sciencedirect.com
SCIENCE DIRECT
Annals of Nuclear Energy 33 (2006) 700–733
annals of NUCLEAR ENERGY
www.elsevier.com/locate/anucene

Nuclear data sensitivity, uncertainty and target accuracy assessment for future nuclear systems

G. Aliberti [a,*], G. Palmiotti [a], M. Salvatores [a], T.K. Kim [a], T.A. Taiwo [a], M. Anitescu [a], I. Kodeli [b], E. Sartori [b], J.C. Bosq [c], J. Tommasi [c]

[a] *Argonne National Laboratory, 9700 S. Cass Ave, Argonne, IL 60439, USA*
[b] *NEA Databank, Paris, France*
[c] *CEA-Cadarache, DER/SPRC Bât. 230, 13108 St-Paul-Lez-Durance, France*

Received 5 December 2005; accepted 2 February 2006
Available online 5 May 2006

Abstract

A sensitivity and uncertainty study has been performed to evaluate the impact of neutron cross-section uncertainty on the most significant integral parameters related to the core and fuel cycle. This work is a contribution to the feasibility assessment of innovative reactor and fuel cycle systems, proposed within the Generation IV initiative. Results of an extensive analysis indicate the most relevant parameters and show any potential significant problems arising from the quality of existing nuclear data, in the assessment of the systems considered. In order to perform these studies, uncertainty covariance data have been produced, mostly based on selected, high accuracy integral experiments. A target accuracy assessment has been also performed in order to evaluate nuclear data improvement requirements. The results of the assessment allows to give guidelines in order to define the most appropriate and effective strategy for data uncertainty reduction.

1. Introduction

A choice of preferred systems for the future has been made, under the auspices of the Gen IV initiative (USDOE, 2002), based on a set of high-level requirements: waste minimization, sustainability, safety, economy, and non-proliferation. At the same time, in the framework of the advanced fuel cycle (AFC) program (US Department of Energy Office of Nuclear Energy, Science, and Technology, 2005), several systems have been considered as possible transmuters of transuranic elements (plutonium, americium, neptunium, curium and higher). The physics of these reactors and their associated fuel cycles is rather well understood. However, their optimization, in order to comply more effectively with the requirements, and their timely deployment, requires focusing the research and development in all fields, in particular for innovative fuel development and processing, and also in the reactor physics field. In this last area, the role of nuclear data are quite significant. Most nuclear data are by and large available in modern data files, but their accuracy and validation is still a major concern.

In order to make a comprehensive assessment, the tools of sensitivity and uncertainty analysis are needed. These tools have been widely developed in the past, in particular for the assessment in the 1970s and 1980s of the performance of fast reactors.

Recently, we performed a preliminary study on the impact of nuclear data uncertainties on the performance parameters (criticality, reactivity coefficients, irradiated fuel isotopic composition, external source effectiveness, etc.), of a generic accelerator driven system, dedicated to

* Corresponding author. Tel.: +1 630 252 7258; fax: +1 630 252 4500.
E-mail address: aliberti@anl.gov (G. Aliberti).

0306-4549/$ - see front matter © 2006 Elsevier Ltd. All rights reserved.
doi:10.1016/j.anucene.2006.02.003

waste transmutation (Aliberti et al., 2004). That study gave indications of the nuclear data uncertainties of relevance and allowed to quantify the requirements for their reduction. In this paper, a much more comprehensive study is presented, devoted to future systems, mainly the ones considered within the Gen IV and AFCI programs, and also for other systems like extended burnup LWRs.

For this type of study, two major difficulties are encountered. First, it is needed to define at an early stage, representative, i.e., general enough, "images" of "future systems". Second, it is necessary to establish a realistic "compilation" of nuclear data uncertainties and their correlation (variance-covariance matrices). Regarding the first point, we have defined what we consider reference "images" of a gas-cooled fast reactor (GFR with full recycling of minor actinides, MA), a sodium-cooled fast reactor (SFR in a transuranics burning configuration with a conversion ratio (CR) <1), a large SFR (referred in the following as EFR) with full recycling of MA and CR ~1, a lead-cooled fast reactor (LFR as defined recently for an IAEA benchmark), and a very high temperature reactor (VHTR) using particulate fuel. Finally, an extended burnup (100 GWd/t) PWR was also studied. On the second point, we started from a first compilation of uncertainties for all the isotopes of interest (actinides, structural, and coolant materials), based as much as possible on the nuclear data performance in the analysis of selected, clean integral experiments (irradiated fuel and sample analysis, criticality and fission rates in zero-power critical facilities) (Palmiotti et al., 2004). For the correlations, we have used the hypothesis of partial energy correlations "by energy band" (PEC). We will call this set of uncertainties (diagonal values) and correlations "ANL Covariance Matrix" (Palmiotti and Salvatores, 2005).

Moreover, a substantial effort has been undertaken at the OECD/NEA DataBank to extract relevant covariance data from current evaluations in major data files and to process them in the same multigroup structure used for sensitivity calculations (Kodeli and Sartori, in preparation). The derived covariance matrix is called "NEA-K Covariance Matrix".

The uncertainty analysis has been applied to a large number of integral parameters which characterize the reference systems indicated above, and their associated fuel cycle: criticality (K_{eff}), temperature and coolant void reactivity coefficients, burnup reactivity swing, spent fuel isotope concentrations indicative of transmutation potential, core power peak, decay heat of the spent fuel in a repository, neutron source arising from the spent fuel e.g., at fuel discharge, and dose (radiotoxicity) of the spent fuel or of the wastes in a repository, at selected times after storage. Based on this uncertainty analysis and on the definition of target accuracies for the various integral parameters, priority requirements for data improvements have been defined. Finally, an approach to define a set of optimized integral experiments in order to reduce uncertainties on the reference systems has been proposed.

2. The approach and theoretical background

2.1. Uncertainties and target accuracies

The approach used for this work includes:

- Sensitivity studies, using the generalized perturbation theory (GPT) (Gandini, 1967), on the selected integral parameters of representative models of the advanced reactor systems.
- Uncertainty assessment using covariance data.

The sensitivity coefficients of an integral parameter R to variations of a nuclear data σ is defined as:

$$S_R = (S_{x,i}) = \left(\begin{vmatrix} S_1 \\ \vdots \\ S_j \\ \vdots \\ S_N \end{vmatrix}_{x,i} \right), \tag{1}$$

where $S_{j,x,i} = \frac{\partial R}{\partial \sigma_{j,x,i}} \cdot \frac{\sigma_{j,x,i}}{R}$ and i, x and j are the indices representing the isotope, the cross-section type and the energy group, respectively.

Once the sensitivity coefficient matrix for each integral parameter R, and the covariance matrix D, defined as:

$$D = (D_{x,i}) = \left(\begin{vmatrix} D_{11} & D_{12} & \cdots & & D_{1N} \\ D_{21} & \cdots & & & \\ \vdots & & D_{\text{jj}} & & \\ & & & \cdots & \\ D_{N1} & & & & D_{\text{NN}} \end{vmatrix}_{x,i} \right), \tag{2}$$

are available, the uncertainty on the integral parameter can be evaluated as follows:

$$\Delta R_0^2 = S_R^+ D S_R. \tag{3}$$

A subsequent step is the assessment of target accuracy requirements.

To establish priorities and target accuracies on data uncertainty reduction, a formal approach can be adopted by defining target accuracies on design parameters and finding out the required accuracy on cross-section data. In fact, the unknown uncertainty data requirements d_l can be obtained (e.g., for parameters l not correlated among themselves), by solving the following minimization problem:

$$\sum_l \lambda_l / d_l^2 = \min, \quad l = 1, \ldots, L. \tag{4}$$

In Eq. (4), L is the total number of parameters with the following constraints:

$$\sum_l S_{nl}^2 d_l^2 < (R_n^T)^2, \quad n = 1, \ldots, N, \tag{5}$$

where N is the total number of integral design parameters, S_{nl} are the sensitivity coefficients for the integral parameter R_n, and R_n^{T} are the target accuracies on the N integral parameters. λ_l are "cost" parameters related to each σ_l and should give a relative figure of merit of the difficulty of improving that parameter (e.g., reducing uncertainties with an appropriate experiment).

2.2. Sensitivity coefficients

Sensitivity coefficients are calculated using GPT methods (Gandini, 1967). A few examples will be given explicitly here.

1. A reactivity coefficient (like the temperature reactivity coefficient) can be expressed as a variation of the reactivity of the unperturbed system (characterized by a value K of the multiplication factor, a Boltzmann operator M, a flux Φ and an adjoint flux Φ^*):

$$\Delta\rho = \left(1-\frac{1}{K_{\mathrm{p}}}\right)-\left(1-\frac{1}{K}\right)=\frac{1}{K}-\frac{1}{K_{\mathrm{p}}}, \tag{6}$$

where K_{p} corresponds to a variation of the Boltzmann operator such that:

$$\begin{aligned} &M \to M_{\mathrm{p}}(=M+\delta M), \quad \underline{\Phi} \to \underline{\Phi}_{\mathrm{p}}(=\underline{\Phi}+\delta\underline{\Phi}_{\mathrm{p}}) \\ &\underline{\Phi}^* \to \underline{\Phi}^*_{\mathrm{p}}(=\underline{\Phi}^*+\delta\underline{\Phi}^*_{\mathrm{p}}), \quad K \to K_{\mathrm{p}}(=K+\delta K_{\mathrm{p}}) \end{aligned} \tag{7}$$

with Φ, Φ_{p}, Φ^* and Φ^*_{p} solutions of:

$$M\underline{\Phi}=\left(A-\frac{1}{K}F\right)\underline{\Phi}=0; \quad M_{\mathrm{p}}\underline{\Phi}_{\mathrm{p}}=\left(A_{\mathrm{p}}-\frac{1}{K_{\mathrm{p}}}F_{\mathrm{p}}\right)\underline{\Phi}_{\mathrm{p}}=0 \tag{8}$$

$$M^*\underline{\Phi}^*=\left(A^*-\frac{1}{K}F^*\right)\underline{\Phi}^*=0; \quad M^*_{\mathrm{p}}\underline{\Phi}^*_{\mathrm{p}}=\left(A^*_{\mathrm{p}}-\frac{1}{K_{\mathrm{p}}}F^*_{\mathrm{p}}\right)\underline{\Phi}^*_{\mathrm{p}}=0 \tag{9}$$

The sensitivity coefficients (at first-order) for $\Delta\rho$ to variations of the σ_j are given as (Gandini et al., 1986):

$$\begin{aligned} S_j &= \frac{\partial(\Delta\rho)}{\partial\sigma_j}\cdot\frac{\sigma_j}{\Delta\rho} \\ &= \frac{1}{\Delta\rho}\left\{\frac{1}{I^{\mathrm{p}}_{\mathrm{f}}}\langle\underline{\Phi}^*_{\mathrm{p}},\ \sigma_{\mathrm{p},j}\underline{\Phi}_{\mathrm{p}}\rangle-\frac{1}{I_{\mathrm{f}}}\langle\underline{\Phi}^*,\ \sigma_j\underline{\Phi}\rangle\right\}, \end{aligned} \tag{10}$$

where $I_{\mathrm{f}}=\langle\underline{\Phi}^*, F\underline{\Phi}\rangle$ and $I^{\mathrm{p}}_{\mathrm{f}}=\langle\underline{\Phi}^*_{\mathrm{p}},\ F_{\mathrm{p}}\underline{\Phi}_{\mathrm{p}}\rangle$, F (or, respectively, F_{p}) being the neutron fission production part of the M $[=A-(1/K)F]$ (or M_{p}) operator; σ_j and σ_{pj} are the same cross-sections in the reference system and in the system characterized by K_{p} and M_{p}, respectively.

2. In the case of nuclide transmutation (i.e., nuclide densities at end of irradiation) the generic nuclide i transmutation during irradiation can be represented as the nuclide density variation between time t_0 and t_{F}. If we denote $n^{\mathrm{i}}_{\mathrm{F}}$ the "final" density for isotope i, the appropriate sensitivity coefficients are given by (Kallfelz et al., 1977):

$$S^i_j=\frac{\partial n^{\mathrm{i}}_{\mathrm{F}}}{\partial\sigma_j}\cdot\frac{\sigma_j}{n^{\mathrm{i}}_{\mathrm{F}}}=\frac{1}{n^{\mathrm{i}}_{\mathrm{F}}}\int_{t_0}^{t_{\mathrm{F}}}\underline{n}^*\sigma_j\underline{n}\,\mathrm{d}t, \tag{11}$$

where the time dependent equations to obtain n and n^* are the classical Bateman equation and its adjoint equation, with appropriate boundary conditions (Kallfelz et al., 1977).

3. In the case of the reactivity loss during irradiation, $\Delta\rho^{\mathrm{cycle}}$, at first order we have:

$$\Delta\rho^{\mathrm{cycle}}=\sum_i\Delta n^{\mathrm{i}}\rho_{\mathrm{i}}, \quad \Delta n^{\mathrm{i}}=n^{\mathrm{i}}_{\mathrm{F}}-n^{\mathrm{i}}_0 \tag{12}$$

and ρ_{i} is the reactivity per unit mass associated with the isotope i.

The related sensitivity coefficients associated with the variation of a σ_j, are given by:

$$\begin{aligned} S^{\mathrm{cycle}}_j &= \frac{\sigma_j}{\Delta\rho^{\mathrm{cycle}}}\cdot\frac{\partial(\Delta\rho^{\mathrm{cycle}})}{\partial\sigma_j} \\ &= \frac{\sigma_j}{\Delta\rho^{\mathrm{cycle}}}\left(\sum_i\frac{\partial n^{\mathrm{i}}}{\partial\sigma_j}\cdot\rho_{\mathrm{i}}+\sum_i\Delta n_{\mathrm{i}}\frac{\partial\rho_{\mathrm{i}}}{\partial\sigma_j}\right) \end{aligned} \tag{13}$$

or

$$\begin{aligned} S^{\mathrm{cycle}}_j &= \sum_i\frac{\rho_{\mathrm{i}}}{\Delta\rho^{\mathrm{cycle}}}\int_{t_0}^{t_{\mathrm{F}}}\underline{n}^*\sigma_j\underline{n}\,\mathrm{d}t \\ &\quad+\frac{1}{\Delta\rho}\left\{\frac{1}{I^{\mathrm{p}}_{\mathrm{f}}}\langle\underline{\Phi}^*_{\mathrm{p}},\ \sigma_{\mathrm{p},j}\underline{\Phi}_{\mathrm{p}}\rangle-\frac{1}{I_{\mathrm{f}}}\langle\underline{\Phi}^*,\ \sigma_j\underline{\Phi}\rangle\right\}. \end{aligned} \tag{14}$$

4. In the case of the power peak, this parameter can be expressed as the ratio:

$$R=\frac{\langle\Sigma_{\mathrm{p}}\underline{\Phi}\rangle_{\mathrm{MAX}}}{\langle\Sigma_{\mathrm{p}}\underline{\Phi}\rangle_{\mathrm{Reactor}}}, \tag{15}$$

with Σ_{p} the power cross-section, essentially represented by $E_{\mathrm{f}}\cdot\Sigma_{\mathrm{f}}$, E_{f} being the average energy released per fission.The sensitivity coefficients are defined as:

$$S_j=\langle\underline{\Psi}^*,\ \sigma_j\underline{\Phi}\rangle \tag{16}$$

and $\underline{\Psi}^*$ is the importance function solution of:

$$M^*\underline{\Psi}^*=\frac{\Sigma_{\mathrm{p,MAX}}}{\langle\Sigma_{\mathrm{p}}\underline{\Phi}\rangle_{\mathrm{MAX}}}-\frac{\Sigma_{\mathrm{p,Reactor}}}{\langle\Sigma_{\mathrm{p}}\underline{\Phi}\rangle_{\mathrm{Reactor}}}, \tag{17}$$

where $\Sigma_{\mathrm{p,MAX}}$ is the Σ_{p} value at the spatial point where $\langle\Sigma_{\mathrm{p}}\underline{\Phi}\rangle\equiv\langle\Sigma_{\mathrm{p}}\underline{\Phi}\rangle_{\mathrm{MAX}}$, and $\Sigma_{\mathrm{p,Reactor}}$ is the Σ_{p} value at each spatial point of the reactor. In Eq. (17), effects due to $\Sigma_{\mathrm{p,MAX}}$ and $\Sigma_{\mathrm{p,Reactor}}$ variations are assumed to be negligible.

5. The final consideration is for the neutron source $\mathrm{NS}_{t=t_{\mathrm{F}}}$ at $t=t_{\mathrm{F}}$ defined as:

$$\mathrm{NS}_{t=t_{\mathrm{F}}}=\sum_i P_{\mathrm{i}}n_{\mathrm{i},t=t_{\mathrm{F}}}, \tag{18}$$

where P_{i} is the neutron production cross-section (e.g., by spontaneous fissions). The sensitivity coefficients are:

$$S^{\mathrm{i}}_j=P_{\mathrm{i}}\cdot\frac{\partial n^{\mathrm{i}}_{\mathrm{F}}}{\partial\sigma_j}\cdot\frac{\sigma_j}{n^{\mathrm{i}}_{\mathrm{F}}}=\frac{P_{\mathrm{i}}}{n^{\mathrm{i}}_{\mathrm{F}}}\int_{t_0}^{t_{\mathrm{F}}}\underline{n}^*\sigma_j\underline{n}\,\mathrm{d}t, \tag{19}$$

where effects due to P_i cross-section variations are supposed to be negligible.

2.3. Calculational tools

All the sensitivity calculations in this study have been performed with the ERANOS code system (Rimpault et al., 2002), which allows to calculate homogeneous and inhomogeneous solutions of the Boltzmann equation and generalized importance functions, and to perform perturbation and uncertainty analysis. Specific modules in ERANOS allow generation of the source terms of the generalized importance equations (see e.g., Eq. (17)) and solution in two or three-dimensional of the finite-difference diffusion or S_n transport equation, or of nodal variational transport equations. A fundamental mode removal algorithm is applied when solving the generalized importance equations for sources that are orthogonal to the homogeneous solutions. Procedures that manipulate different perturbation modules are used to generate the sensitivity coefficients related to reactivity coefficients (see Eq. (10)). Uncertainty evaluation (see Eq. (3)) and representativity factors (see Section 8) are computed in ERANOS with covariance matrices provided in different general formats.

The discrete ordinate module BISTRO (Palmiotti et al., 1990) in ERANOS has been used to perform flux and generalized importance function calculations. An S_4P_1 approximation in RZ geometry has been proved accurate enough for this type of calculation. In order to avoid problems related to S_n negative solutions that are present for instance in the case of reaction rate ratios importance calculations, ERANOS uses a special procedure that allows separately calculating the generalized importance for the positive and negative contributions and combining them at the level of the perturbation or sensitivity coefficient computation (Palmiotti and Salvatores, 1988).

Decay heat calculations have been performed with the ORIGEN code (Bell, 1973). The time dependent perturbation calculations are performed using the NUTS code (Palmiotti et al., 1994). NUTS solves the direct and adjoint time dependent Bateman equations and computes the perturbation integrals of Eqs. (11) and (19), taking into account power plant history and reprocessing losses for any type of nuclear fuel cycle. NUTS can also compute inhomogeneous solutions of the adjoint equations that are used for sensitivity calculations of time integrated quantities (e.g., time integrated decay heat in a nuclear waste repository).

3. The covariance data

The "ANL covariance matrix" (Palmiotti and Salvatores, 2005), was obtained by updating the covariance matrix used in the ADS study (Aliberti et al., 2004) by taking into account mainly the results of clean integral experiment analysis, in particular irradiated sample/fuel analysis, which gave valuable information on capture and some $(n, 2n)$ cross-sections, and of fission rate measurements in critical assemblies (see Section 3.1). It should be stressed that these variance-covariance data are "plausible but hypothetical" (Smith, 2005) and they are a preliminary step towards a sound evaluation of covariances using e.g. the approach suggested by Smith (2004) and Koning (2004), where Monte-Carlo techniques are applied to vary randomly nuclear model parameters within ranges defined by their estimated uncertainties.

The uncertainty values, have been given by "energy band", consistent with the multigroup energy structures used for deterministic calculations both of thermal and fast reactors. Fifteen energy groups have been selected between 20 MeV and thermal energy. Two extra groups between 150 and 20 MeV are related to ADS applications. In the resonance range, the uncertainties are for broad energy-average cross-sections, and do not apply to individual resonances. The uncertainty values are given only for neutron cross-section data of actinides and structural materials. Fission products related uncertainties are treated separately. We will revisit this specific point (see Section 3.2).

3.1. Actinide isotope data uncertainties

In establishing uncertainties and covariances for uranium (U) and transuranics (TRU) multigroup nuclear data using integral experiment analysis, one can distinguish among four classes of isotopes:

(a) major isotopes (i.e., U-235, U-238, and Pu-239);
(b) other U and Pu isotopes (e.g., U-234, U-236, Pu-238, Pu-240, Pu-241, and Pu-242);
(c) minor actinides up to Cm-245 (i.e., Np-237, Am-241, Am-242, Am-243, Cm-242, Cm-244, and Cm-245);
(d) higher mass minor actinides.

For class (a) isotopes, uncertainty estimates from the analysis of a large set of integral experiments databases in the thermal energy range have been attempted in several laboratories (e.g., Courcelle et al., 2004; Marcian et al., 2004; Trakas and Dandin, 2004). Only few values, e.g., related to $(n, 2n)$ data can be controversial, and a general consensus can be expected on the values which we have assembled in the ANL covariance matrix. As examples, we show the U-235 data in Table 1, for which we have taken into account the recent work by Lubitz (2004), and the U-238 data in Table 2.

For classes (b) and (c) isotopes, the integral database is also relevant, although recent analytical studies have concentrated on data of relevance for thermal neutron systems (Courcelle et al., 2004; Marcian et al., 2004; Trakas and Dandin, 2004); and we have based our estimates on these studies. Practically, no uncertainty assessment exists for isotopes of class (d).

Since a large number of Gen IV systems are characterized both by a fast spectrum and by the presence in the core

Table 1
U-235 standard deviations (%)

Gr	Energy	U-235					
		ν	σ_f	σ_{inel}	σ_{el}	σ_{capt}	$\sigma_{n,2n}$
1	150 MeV	3	10	30	15	30	100
2	55.2 MeV	2	10	20	10	20	100
3	19.6 MeV	1	5	10	5	15	50
4	6.07 MeV	1	5	10	5	15	50
5	2.23 MeV	1	5	10	5	15	
6	1.35 MeV	1	5	15	5	15	
7	498 keV	1	5	15	5	15	
8	183 keV	1	5	15	5	15	
9	67.4 keV	1	5	20	5	10	
10	24.8 keV	1	5	25	5	10	
11	9.12 keV	1	5	25	5	5	
12	2.03 keV	0.5	3	30	5	5	
13	454 eV	0.5	3		5	5	
14	22.6 eV	0.5	3		5	5	
15	4.00 eV	0.5	3		5	3	
16	0.54 eV	0.5	1		5	1	
17	0.10 eV	0.3	1		5	1	

Table 2
U-238 standard deviations (%)

Gr	Energy	U-238					
		ν	σ_f	σ_{inel}	σ_{el}	σ_{capt}	$\sigma_{n,2n}$
1	150 MeV	3	10	30	15	30	100
2	55.2 MeV	2	10	20	10	20	100
3	19.6 MeV	3	5	20	5	30	30
4	6.07 MeV	2	5	15	5	10	
5	2.23 MeV	2	5	10	5	5	
6	1.35 MeV	2	5	10	5	5	
7	498 keV	2	5	10	5	5	
8	183 keV	2	20	10	5	5	
9	67.4 keV	2	20	15	5	5	
10	24.8 keV	2	20		5	5	
11	9.12 keV	2	20		5	3	
12	2.03 keV	2	20		5	3	
13	454 eV	2	20		5	3	
14	22.6 eV	2	20		5	3	
15	4.00 eV	2	20		5	3	
16	0.54 eV	2	20		1	1	
17	0.10 eV	2	20		1	1	

of recycled MAs, it was felt essential to use high accuracy integral experiments in the fast energy range to provide guidance in establishing realistic uncertainty estimates in the "fast" energy range for isotopes of classes (a)–(c). Special emphasis was put on the series of fuel (TRAPU experiments) and sample (PROFIL experiments) irradiations in the PHENIX reactor, and their detailed analysis (Palmiotti et al., 2004). For these experiments, the observed calculation-to-experiment (C/E) discrepancies, can be mostly interpreted in terms of capture cross-section and $(n, 2n)$ data. Table 3 shows results for the PROFIL experiments, expressed as C/E on the energy integral of selected cross-sections, and Table 4 shows results for the TRAPU experiments, expressed as C/E on the isotope concentrations at the end of irradiation. Only a few cases among those shown

Table 3
PROFIL experiment C/E

		PROFIL-1		PROFIL-2	
		C/E	Uncertainty (%)	C/E	Uncertainty (%)
σ_c	U-235	0.98	1.7	0.99	1.7
$\sigma_{n,2n}$	U-235	0.76	5.0	0.68	5.0
σ_c	U-238	0.99	2.3	1.01	2.3
σ_c	Pu-238	0.96	4.0	0.98	4.0
σ_c	Pu-239	0.96	3.0	0.96	3.0
$\sigma_{n,2n}$	Pu-239	0.97	15.0	0.74	15.0
σ_c	Pu-240	1.00	2.2	0.97	2.2
σ_c	Pu-241	1.01	4.1	–	–
σ_c	Pu-242	1.18	3.5	–	–
σ_c	Am-241	1.05	1.7	1.05	1.7
σ_c	Am-243	0.99	5.0	–	–
σ_c	Np-237	–	–	0.95	3.6

Calculation performed with JEFF3.0 data.

in Tables 3 and 4, would require accounting for systematic uncertainties. For most cases, the C/E values are close to the experimental uncertainty of the related data at least in an integral sense.

The knowledge of the sensitivity contribution of different data in a specific experiment (see e.g., Tables 5 and 6 relative to the TRAPU-2 experiment) and of the energy sensitivity profile of the experiment to the dominating data (e.g., capture cross-section, for single isotope sample irradiation, see Fig. 1), allows us to distribute on the multigroup data the integral information on the uncertainty. This process has been used to assess uncertainty estimates for the capture (and a few $n, 2n$) cross-sections of classes (a)–(c) isotopes in the range ~5 MeV down to ~500 eV.

For inelastic and fission cross-section data, critical mass zero-power experiments and fission rate ratios in fast critical assemblies have also been used (Palmiotti et al., 2004) to complement the irradiation experiments previously mentioned in order to deduce uncertainties for the ANL covariance data set.

As an example of a class (b) isotope, the Pu-240 diagonal uncertainty data are given in Table 7.

3.2. Fission product data uncertainty

The status of fission product (FP) neutron cross-section evaluation has been assessed recently (Obložinský, 2005), but no uncertainty estimates were given.

In the present version of the ANL covariance data, it was not attempted to establish detailed uncertainty data for all significant isotopes. However, an uncertainty estimate is possible in an integral sense, based once more on integral experiment analysis. A previous work in this direction is described by Gruppelaar (1998).

In the case of fast reactors some of the most important fission products (in terms of contribution to the FP component of the reactivity loss/cycle) have been irradiated as pure, separated isotopes in PHENIX, during the PROFIL experiments mentioned previously. Relevant information

Table 4
C/E values of final concentrations in the TRAPU experiments

Isotope	TRAPU-1		TRAPU-2		TRAPU-3	
	C/E[a]	Experimental uncertainity (%)	C/E[a]	Experimental uncertainity (%)	C/E[a]	Experimental uncertainity (%)
U-234	0.98	±3.9	1.00	±3.8	1.04	±4.6
U-235	1.01	±0.4	1.03	±0.4	1.02	±0.4
U-236	0.96	±0.8	0.98	±1.0	0.98	±0.9
Np-237	0.86	±6.8	0.85	±3.3	0.81	±3.2
Pu-238	1.00	±1.5	1.00	±1.0	1.02	±1.6
Pu-239	1.02	±0.6	1.00	±0.5	1.00	±0.4
Pu-240	1.00	±0.6	0.98	±0.6	1.00	±0.6
Pu-241	1.01	±0.6	0.99	±0.6	1.00	±0.6
Pu-242	1.05	±0.8	1.01	±0.6	1.01	±0.6
Am-241	0.95	±3.2	0.97	±3.9	0.97	±2.6
Am-242m	1.02	±3.8	1.06	±4.3	1.04	±3.1
Am-243	1.04	±2.6	1.01	±3.1	1.05	±2.5
Cm-242	1.01	±3.9	0.99	±3.1	0.99	±2.7
Cm-243	–	–	0.67	±3.1	0.68	±3.2
Cm-244	0.98	±2.1	1.10	±2.3	1.12	±1.8

[a] JEF3.0 data used in the calculations.

Table 5
Sensitivity (% variation) of isotope build-up for 100% variation of selected basic data

Basic data	Isotope build-up						
	U-234	U-235	U-236	Np-237	Pu-238	Pu-239	Pu-240
U-234 σ_{cap}	−10	0.2					
U-234 σ_{fis}	−6						
U-235 σ_{cap}		−10.8	90	9.7	0.2		
U-235 σ_{fis}	−0.2	−36.2	−16.2	−1.2			
U-236 σ_{cap}			−5.7	10.5	0.2		
U-238 σ_{cap}				−2.3		26.7	3.9
U-238 σ_{fis}				−0.4		−0.1	
U-238 $\sigma_{(n,2n)}$	0.1			82.5	1.8		
Np-237 σ_{cap}	0.2			−14.0	1.9		
Np-237 σ_{fis}				−3.1			
Pu-238 σ_{cap}	−1.1				−8.0		
Pu-238 σ_{fis}	−2.1				−16.9		
Pu-239 σ_{cap}			0.2			−8.1	26.2
Pu-239 σ_{fis}						−29.4	−4.3
Pu-240 σ_{cap}			−0.1	0.1	0.4		−9.3
Pu-240 σ_{fis}			−0.1				−6.7
Pu-241 σ_{cap}					−0.1		
Pu-241 σ_{fis}				−0.1	−0.6		
Pu-242 σ_{cap}							
Pu-242 σ_{fis}							
Am-241 σ_{cap}	2.7			−0.7	26.1		
Am-241 σ_{fis}					−0.7		
Am-242m σ_{fis}							
Am-243 σ_{cap}							
Am-243 σ_{fis}							
Cm-242 σ_{cap}					−0.7		
Cm-242 σ_{fis}					−0.8		
Cm-243 σ_{fis}							

Case of TRAPU-2 experiment.

on the capture cross-section of those isotopes has been obtained with the analysis of these experiments. Results are shown in Table 8 for the PROFIL-1 experiments. These results are confirmed by an independent analysis (Tommasi et al., in press), which has been extended to some other FP isotopes, irradiated as part of the PROFIL-2 experiment. In view of the C/E values observed and of the experimental uncertainties quoted for the experiments (and shown in Table 8), an overall uncertainty of ±10% can be associated with the capture

Table 6
Sensitivity (% variation) of isotope build-up for 100% variation of selected basic data

Basic data	Isotope build-up							
	Pu-241	Pu-242	Am-241	Am-242m	Am-243	Cm-242	Cm-243	Cm-244
U-234 σ_{cap}								
U-234 σ_{fis}								
U-235 σ_{cap}								
U-235 σ_{fis}								
U-236 σ_{cap}								
U-238 σ_{cap}	0.6							
U-238 σ_{fis}								
U-238 $\sigma_{(n,2n)}$								
Np-237 σ_{cap}								
Np-237 σ_{fis}								
Pu-238 σ_{cap}								
Pu-238 σ_{fis}								
Pu-239 σ_{cap}	5.7	0.4	0.6	0.1	0.2	0.2		
Pu-239 σ_{fis}	−0.7		−0.2					
Pu-240 σ_{cap}	30.5	3.5	4.4	1.5	1.7	2.0	1.2	0.8
Pu-240 σ_{fis}	−1.2	−0.1	−0.1					
Pu-241 σ_{cap}	−8.8	24.2	−1.4	−0.5	15.5	−0.7	−0.4	10.7
Pu-241 σ_{fis}	−40.7	−5.4	−6.7	−2.4	−2.5	−3.2	−1.8	−1.2
Pu-242σ_{cap}		−7.7			93.8		−0.1	95.4
Pu-242 σ_{fis}		−4.6			−2.4			−1.8
Am-241 σ_{cap}		2.8	−30.5	82.1	3.3	77.7	85.4	2.8
Am-241 σ_{fis}			−4.7	−2.8	−0.1	−3.4	−2.2	
Am-242m σ_{fis}				−27.1	−0.3			−0.2
Am-243 σ_{cap}					−15.2		0.2	89.7
Am-243 σ_{fis}					−1.8			−1.4
Cm-242 σ_{cap}						−3.1	97.7	0.5
Cm-242 σ_{fis}						−3.7	−2.6	
Cm-243 σ_{fis}							−20.6	

Case of TRAPU-2 experiment.

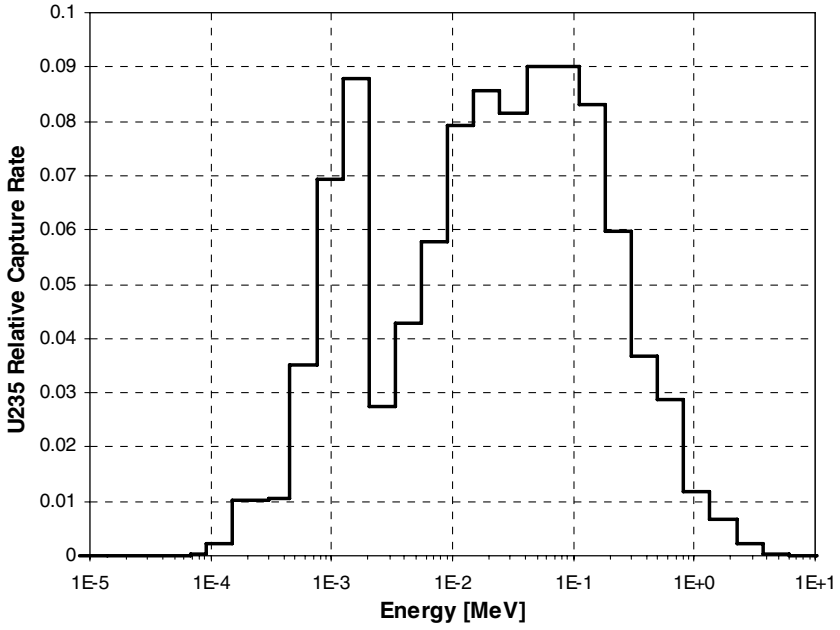

Fig. 1. PHENIX U-235 normalized capture rate by group.

cross-section of a "lumped" FP, defined as: $\sigma^{lumped} = \Sigma\gamma_n\sigma_n$, where γ_n is the effective yield of fission product n. This estimate is higher than the one given by Gruppelaar (1998), but in our opinion justified by the observed C/E values shown above. The uncertainty associated with the scattering (inelastic + elastic) cross-section of a "lumped"

Table 7
Pu-240 standard deviations (%)

Gr	Energy	Pu-240					
		ν	σ_f	σ_{inel}	σ_{el}	σ_{capt}	$\sigma_{n,2n}$
1	150 MeV	3	15	45	30	90	100
2	55.2 MeV	3	15	30	20	60	100
3	19.6 MeV	3	5	15	10	20	100
4	6.07 MeV	2	5	15	10	20	
5	2.23 MeV	2	5	15	10	20	
6	1.35 MeV	2	5	15	10	20	
7	498 keV	2	5	20	10	20	
8	183 keV	2	5	20	10	20	
9	67.4 keV	2	5	25	10	20	
10	24.8 keV	2	5		10	10	
11	9.12 keV	2	10		10	10	
12	2.03 keV	2	10		10	10	
13	454 eV	2	10		10	10	
14	22.6 eV	2	10		10	10	
15	4.00 eV	2	10		10	7	
16	0.54 eV	2	50		5	3	
17	0.10 eV	2	50		5	2	

Table 9
Fe-56 standard deviations (%)

Gr	Energy	Fe56			
		σ_{inel}	σ_{el}	σ_{capt}	$\sigma_{n,2n}$
1	150 MeV	100	60	60	100
2	55.2 MeV	80	40	40	100
3	19.6 MeV	20	30	45	100
4	6.07 MeV	15	20	30	
5	2.23 MeV	10	10	15	
6	1.35 MeV	20	10	10	
7	498 keV		10	8	
8	183 keV		10	8	
9	67.4 keV		8	8	
10	24.8 keV		6	8	
11	9.12 keV		4	8	
12	2.03 keV		4	8	
13	454 eV		4	8	
14	22.6 eV		4	8	
15	4.00 eV		4	8	
16	0.54 eV		4	8	
17	0.10 eV		4	8	

Table 8
PROFIL-1 C/E's for selected fission product samples

Data type	C/E[a]	Experimental uncertainity (%)
σ_{capt} Mo-95	1.08	3.8
σ_{capt} Mo-97	1.00	4.4
σ_{capt} Ru-101	1.06	3.6
σ_{capt} Pd-105	0.87	4.0
σ_{capt} Cs-133	0.95	4.7
σ_{capt} Nd-145	1.17	3.8
σ_{capt} Sm-149	0.97	3.1

[a] JEF3.0 data used in the calculations.

FP is ±20%, which seems to be justified also by the work by Gruppelaar (1998) and Kawai (2002).

Finally, as far as the existing thermal neutron systems, systematic studies performed mainly at the CEA indicated an overall uncertainty of the order of ±2% on a lumped fission product capture cross-section, which derives mostly from the experience on the burnup reactivity in PWRs (Santamarina, 2005).

3.3. Structural and coolant materials

Only a few uncertainty evaluations are available in existing data files for selected isotopes. These evaluations have been used in particular for Fe-56, together with estimations of uncertainties mainly based on the inspection of discrepancies among available data files. This procedure is certainly a very preliminary attempt to establish uncertainties for the cross-sections of these isotopes. However, for some relevant cases, like Pb cross-sections at high energy or Fe-56 cross-sections above 100 eV, fairly realistic estimates can be defined. As an example, the Fe-56 data are shown in Table 9.

3.4. Energy correlation

In the previous sections, we have indicated the rationale followed to establish the diagonal values of the variance-covariance matrices for the different types of isotope cross-sections.

In a second step, partial energy correlations were introduced. The same correlations for all isotopes and reactions have been used, under the form of full energy correlation in 5 energy bands. The idea was to single out energy regions of relevance, in particular for actinides:

1. the region above the threshold of fertile isotope fission cross-sections, and of many inelastic cross-sections, up to 20 MeV;
2. the region of the continuum down to the upper unresolved resonance energy limit;
3. the unresolved resonance energy region;
4. the resolved resonance region;
5. the thermal range.

The correlations used are shown in Fig. 2. No correlation among different reactions or different isotopes has been considered at this stage. This assumption may lead to non-conservative results in some cases.

3.5. Evaluated covariance matrices

As indicated in the introduction, available covariance data at the NEA DataBank (Kodeli and Sartori, in preparation) have also been used, mainly to provide a comparison with the ANL Covariance Data. The comparison cannot be complete, but limited to selected isotopes and reactions, since some data used in this analysis, are missing in the available evaluated covariance data. The data

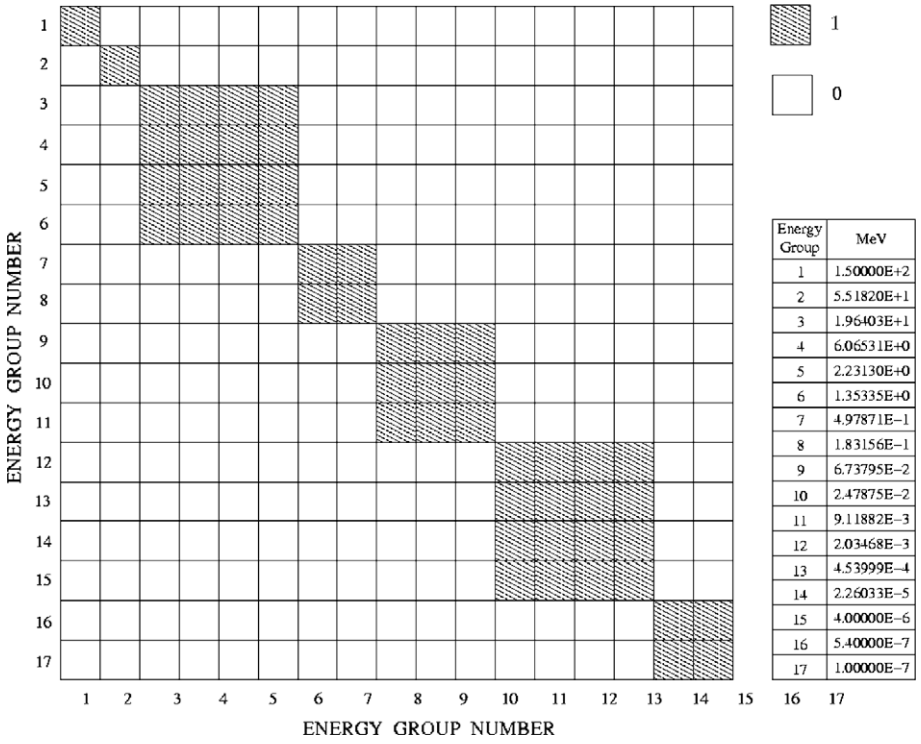

Energy Group	MeV
1	1.50000E+2
2	5.51820E+1
3	1.96403E+1
4	6.06531E+0
5	2.23130E+0
6	1.35335E+0
7	4.97871E−1
8	1.83156E−1
9	6.73795E−2
10	2.47875E−2
11	9.11882E−3
12	2.03468E−3
13	4.53999E−4
14	2.26033E−5
15	4.00000E−6
16	5.40000E−7
17	1.00000E−7

Fig. 2. Energy correlations used in the ANL correlation matrix (PEC).

Table 10
NEA-K covariance matrix

U-235	ν, fission, inelastic, elastic, (n, γ), $(n, 2n)$	JENDL3.3
U-238	ν, inelastic, elastic, $(n, 2n)$	JENDL3.3
	Fission, (n, γ)	IRDF-2002
Np-237	Fission	IRDF-2002
Pu-239	ν, inelastic, elastic, (n, γ), $(n, 2n)$	JENDL3.3
	Fission	IRDF-2002
Pu-240	Inelastic, elastic, fission, (n, γ), $(n, 2n)$	JENDL3.3
Pu-241	ν, inelastic, elastic, fission, (n, γ), $(n, 2n)$	JENDL3.3
Am-241	Fission	IRDF-2002
C	Elastic, (n, γ)	ENDF/B-V
H	Elastic, (n, γ)	ENDF/B-V
O	Inelastic, elastic	ENDF/B-V
Cr-52	Inelastic, elastic, capture, $(n, 2n)$	ENDF/B-VI
Fe-56	Inelastic, elastic, capture, $(n, 2n)$	ENDF/B-VI
Na-23	Inelastic, elastic, capture, $(n, 2n)$	ENDF/B-VI
Pb-206	Inelastic, elastic, (n, γ), $(n, 2n)$	ENDF/B-VI
Pb-207	Inelastic, elastic, (n, γ), $(n, 2n)$	ENDF/B-VI
Pb-208	Inelastic, elastic, (n, γ), $(n, 2n)$	ENDF/B-VI
Si	Inelastic, elastic, (n, p), (n, α)	ENDF/B-VI
Zr-90	Inelastic, (n, γ), $(n, 2n)$	JENDL3.3
B-10	(n, α)	IRDF-2002
Ni-58	Inelastic, elastic, capture, $(n, 2n)$	JEFF3

Origin of the data.

selected (NEA-K Covariance Matrix) are shown in Table 10. Ideally, the covariance data should be taken from a single evaluation, i.e., the one used in the calculations, in order to assure the consistency among the nuclear data used. At present no evaluation is complete enough to cover all the materials needed in this study and the NEA-K covariance matrices are therefore a selection (more or less consistent) of the data available in the ENDF/B-V, ENDF/B-VI, IRDF-2002, JENDL-3.3 and JEFF-3 evaluations.

In addition, inconsistencies were found in some evaluated covariances, like unrealistically low standard deviations or omitted values at some energy ranges, indicating the need for further improvements in the covariance data evaluations. The following matrices contain zero or very low standard deviations:

- Pu-241 (reactions (n, f) and (n, γ), see Fig. 5).
- Pu-240 (n, γ), (Fig. 4).
- Pu-239 (n, γ), (around 1 keV).
- U-235 total, elastic (n, f), (n, γ) (below 20 keV).

For some isotopes (in particular Pu-241) low variances appear in the energy ranges where the cross-section values are not small therefore the corresponding data should be used with caution.

Some comparisons of the ANL and NEA-K covariance matrices for selected isotopes and reactions are given in Figs. 3–6.

A few relevant features can be underlined:

1. For some major isotope reactions (like Pu-239 σ_f), the diagonal values of the estimated ANL covariance data are fairly close to specifically evaluated data. This is the case also of U-238 σ_c, U-235 σ_f, etc.

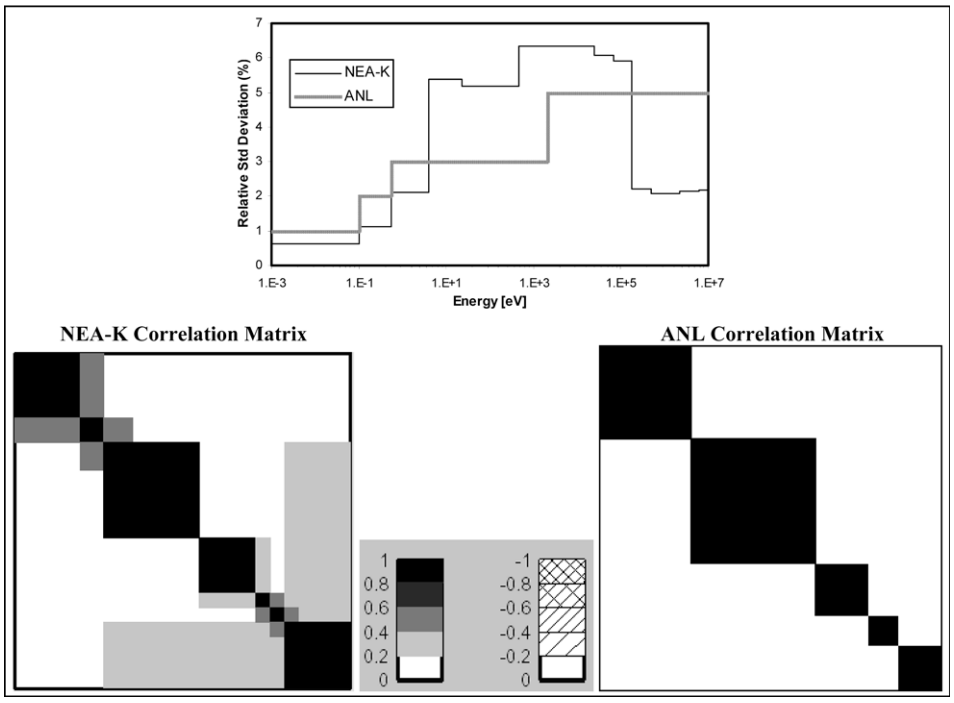

Fig. 3. Comparison of correlation matrices for Pu-239 (n, f).

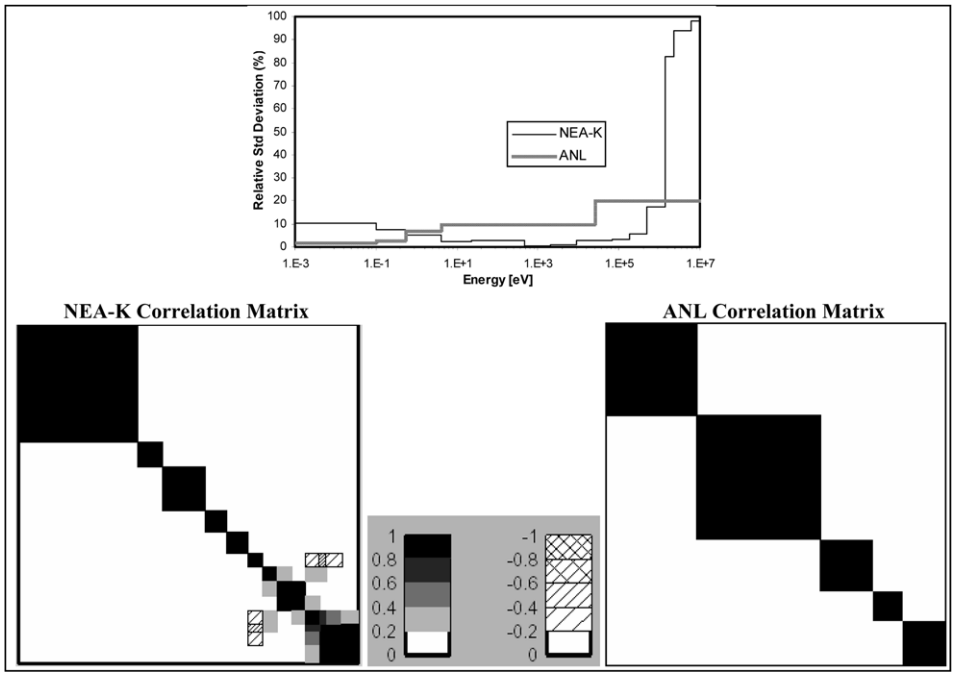

Fig. 4. Comparison of correlation matrices for Pu-240 (n, γ).

2. As far as "diagonal" values for some class (b) and class (c) isotopes, the evaluated data uncertainties look extremely low and not consistent with the performance of data in integral experiment analysis, as shown previously.
3. As far as "off-diagonal" values, there is, at least qualitatively a remarkable similarity in many cases between the evaluated data and the estimated covariances "by energy band" as implemented by Palmiotti and Salvatores (2005).

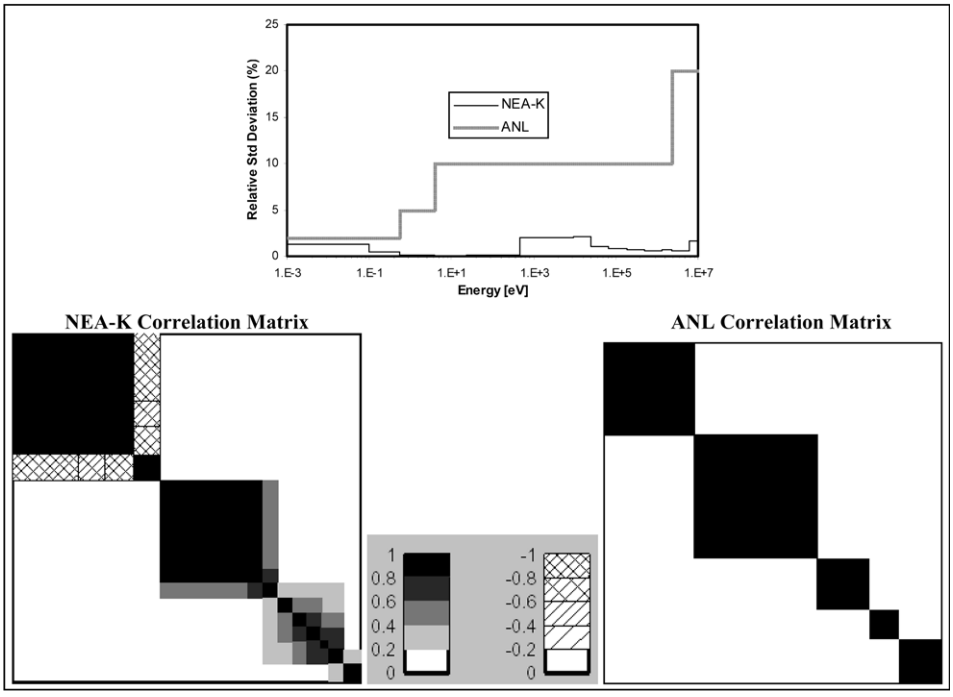

Fig. 5. Comparison of correlation matrices for Pu-241 (n, f).

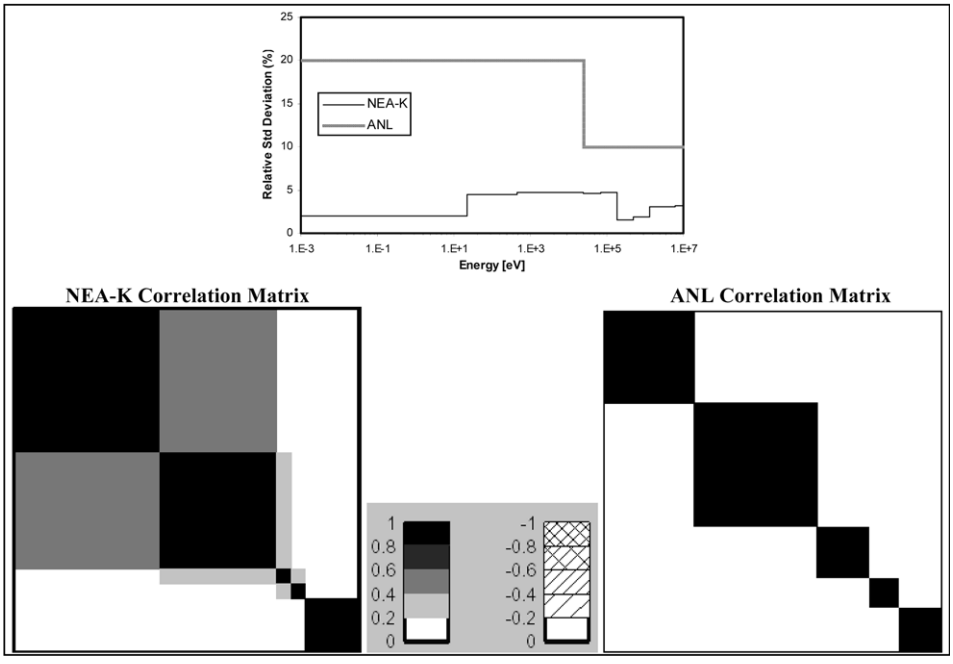

Fig. 6. Comparison of correlation matrices for Am-241 (n, f).

4. The systems used in the analysis

As indicated in the Introduction, six systems, related to the Gen IV and AFCI programs, have been considered.

1. GFR: 2400 MW_e – He cooled; SiC – (U-TRU)C fuel; Zr_3Si_2 reflector; Pu content: 17%, MA content: 5%; irradiation cycle: 415 d.
2. LFR: 900 MW_{th} – Pb cooled; U-TRU-Zr metallic alloy fuel; Pb reflector; Pu content: 21%, MA content: 2%; irradiation cycle: 310 d.
3. SFR (Burner: CR = 0.25): 840 MW_{th} – Na cooled; U-TRU-Zr metallic alloy fuel; SS reflector; Pu content: 56%, MA content: 10%; irradiation cycle: 155 d.
4. EFR: 3600 MW_{th} – Na cooled; U-TRU oxide fuel; U blanket; Pu content: 22.7%, MA content: 1%; irradiation cycle: 1700 d.

5. VHTR: TRISO fuel; U-235 enrichment: 14%; burnup: 90 GW d/kg.
6. Extended BU PWR: U-235 enrichment: 8.5%; burnup: 100 GW d/kg.

The average core compositions for the different systems are presented in Tables 11 and 12, and the core geometry details are given in Fig. 7.

The calculations were performed with the ERANOS code system (Rimpault et al., 2002) and the JEFF3.0 library (OECD/NEA Data Bank, 2005). The neutron spectra and adjoint fluxes at the core center of the systems are shown in Figs. 8–19.

The parameters considered in the sensitivity and uncertainty analysis are:

- Criticality (multiplication factor).
- Peak power value.
- Temperature reactivity coefficient.
- Coolant void reactivity coefficient.
- Reactivity loss during irradiation.
- Transmutation potential (i.e., nuclide concentrations at end of irradiation).
- Decay heat in a repository (at 100 years after disposal).
- Neutron source at two years after fuel discharge.
- Radiotoxicity at $t = 100{,}000$ years after disposal.

Nominal values calculated for each reactor are summarized in Tables 13–15.

5. Uncertainty analysis

5.1. Uncertainty evaluation

A summary of the uncertainty results obtained with the ANL Covariance Matrix (both without correlations and with partial energy correlations, PEC) is shown in Tables 16–18.

For the burnup reactivity ($\Delta\rho$) swing, the uncertainty values quoted in Tables 16–18 are due only to the uncertainties in the actinide cross-sections. For the fission product component, we have used the "lumped" fission product cross-section uncertainty as defined in Section 3.2. Using the breakdown of the $\Delta\rho$ into components shown in Table 19 for the different systems, an uncertainty evaluation was performed on the fission product reactivity component as

Table 11
Average core compositions (10^{24} at/cm^3)

GFR			LFR			SFR		
Isotope	BOC	EOC	Isotope	BOC	EOC	Isotope	BOC	EOC
U-234	5.041E−15	3.515E−7	U-234	1.035E−5	1.025E−5	U-234	1.545E−5	1.531E−5
U-235	3.323E−5	2.829E−5	U-235	7.754E−6	7.182E−6	U-235	5.030E−6	4.890E−6
U-236	5.041E−15	1.163E−6	U-236	2.698E−5	2.659E−5	U-236	1.119E−5	1.109E−5
U-238	4.715E−3	4.613E−3	U-238	4.686E−3	4.623E−3	U-238	1.697E−3	1.677E−3
Np-237	4.939E−5	4.430E−5	Np-237	3.436E−5	3.251E−5	Np-237	8.626E−5	8.125E−5
Pu-238	3.673E−5	4.503E−5	Pu-238	5.432E−5	5.380E−5	Pu-238	1.414E−4	1.382E−4
Pu-239	4.855E−4	4.996E−4	Pu-239	6.332E−4	6.181E−4	Pu-239	7.325E−4	6.862E−4
Pu-240	3.026E−4	3.031E−4	Pu-240	4.592E−4	4.501E−4	Pu-240	8.822E−4	8.589E−4
Pu-241	8.362E−5	7.431E−5	Pu-241	5.229E−5	5.183E−5	Pu-241	1.610E−4	1.533E−4
Pu-242	1.050E−4	1.051E−4	Pu-242	8.888E−5	8.751E−5	Pu-242	2.726E−4	2.674E−4
Am-241	1.855E−4	1.640E−4	Am-241	5.521E−5	5.203E−5	Am-241	1.069E−4	1.019E−4
Am-242m	7.007E−7	3.486E−6	Am-242m	3.702E−6	3.701E−6	Am-242m	7.408E−5	6.561E−5
Am-243	4.597E−5	4.379E−5	Am-243	2.652E−5	2.608E−5	Am-243	9.517E−5	9.384E−5
Cm-242	5.041E−8	7.094E−6	Cm-242	1.675E−6	2.150E−6	Cm-242	5.827E−6	6.134E−6
Cm-243	2.067E−7	3.045E−7	Cm-243	1.338E−7	1.398E−7	Cm-243	5.688E−7	5.612E−7
Cm-244	1.504E−5	1.829E−5	Cm-244	1.722E−5	1.754E−5	Cm-244	6.698E−5	6.747E−5
Cm-245	3.680E−6	3.571E−6	Cm-245	5.066E−6	4.769E−6	Cm-245	1.738E−5	1.663E−5
Cm-246	2.823E−7	3.450E−7	Cm-246	2.938E−6	2.910E−6	Cm-246	9.456E−6	9.336E−6
FP[a]	3.041E−14	2.147E−4	FP[a]	2.223E−4	4.136E−4	FP[a]	4.126E−4	6.631E−4
He-4	2.140E−4	2.140E−4	Zr	3.830E−3	3.830E−3	Fe	2.061E−2	2.061E−2
Si	1.218E−2	1.218E−2	Pb	1.674E−2	1.674E−2	Cr	2.994E−3	2.994E−3
C	1.824E−2	1.824E−2	Fe	8.632E−3	8.632E−3	Ni	1.153E−4	1.153E−4
			Ni	4.831E−5	4.831E−5	Mo	2.117E−4	2.117E−4
			Cr	1.254E−3	1.254E−3	Zr	2.478E−3	2.478E−3
			Mo	8.867E−5	8.867E−5	Na	1.099E−2	1.099E−2
			Mn	9.291E−5	9.291E−5	Mn	2.218E−4	2.218E−4
			B-10	2.019E−4	2.019E−4			
			B-11	2.172E−4	2.172E−4			
			C	1.217E−4	1.217E−4			
			Li-7	6.782E−5	6.782E−5			

[a] Fission products.

Table 12
Average core compositions (10^{24} at/cm^3)

EFR					VHTR inner, central and outer fuel			PWR		
Isotope	Fuel		Blanket		Isotope	BOC	EOC	Isotope	BOC	EOC
	BOC	EOC	BOC	EOC						
U-234	9.517E−6	7.239E−6	6.577E−8	5.542E−8	U-235	2.492E−5	1.088E−5	U-233	–	1.112E−12
U-235	5.975E−6	3.357E−6	8.748E−6	5.322E−6	U-238	1.511E−4	1.414E−4	U-234	–	1.331E−7
U-236	6.585E−6	6.347E−6	2.798E−6	3.273E−6	Np-237	–	1.479E−7	U-235	5.721E−4	6.398E−5
U-238	6.613E−3	5.701E−3	9.555E−3	8.951E−3	Pu-238	–	4.856E−8	U-236	–	8.305E−5
Np-237	9.356E−6	8.880E−6	1.089E−14	1.268E−6	Pu-239	–	2.518E−6	U-237	–	1.138E−7
Pu-238	3.902E−5	3.561E−5	1.084E−14	2.887E−7	Pu-240	–	7.565E−7	U-238	6.159E−3	5.759E−3
Pu-239	1.109E−3	8.623E−4	1.079E−14	4.211E−4	Pu-241	–	8.910E−7	Np-237	–	9.534E−6
Pu-240	6.633E−4	6.015E−4	1.075E−14	4.081E−5	Pu-242	–	2.356E−7	Np-239	–	5.805E−7
Pu-241	6.598E−5	8.287E−5	1.070E−14	3.299E−6	Am-241	–	2.070E−8	Pu-238	–	7.042E−6
Pu-242	7.264E−5	6.870E−5	1.066E−14	1.621E−7	Am-242m	–	4.244E−10	Pu-239	–	5.070E−5
Am-241	5.991E−5	3.354E−5	1.070E−14	2.032E−7	Am-243	–	3.379E−8	Pu-240	–	2.523E−5
Am-242m	2.974E−6	3.073E−6	1.066E−14	3.787E−9	Cm-242	–	7.584E−9	Pu-241	–	1.706E−5
Am-243	1.685E−5	1.745E−5	1.062E−14	6.707E−9	Cm-243	–	1.343E−10	Pu-242	–	1.043E−5
Cm-242	7.985E−9	2.774E−6	1.066E−14	8.353E−9	Cm-244	–	8.067E−9	Cm-242	–	3.530E−7
Cm-243	4.087E−7	3.707E−7	1.062E−14	3.101E−10	Cm-245	–	4.298E−10	Cm-243	–	1.506E−8
Cm-244	1.217E−5	1.554E−5	1.057E−14	8.114E−10	C	6.400E−2	6.400E−2	Cm-244	–	2.240E−6
Cm-245	2.816E−6	2.577E−6	1.053E−14	3.483E−11	O	2.641E−4	2.641E−4	Cm-245	–	2.227E−7
Cm-246	1.776E−6	1.544E−6	1.049E−14	6.773E−13	Si	5.228E−4	5.228E−4	O	2.744E−2	2.744E−2
Cm-247	1.893E−7	2.583E−7	1.044E−14	2.496E−14				H	2.794E−2	2.794E−2
Cm-248	1.107E−7	1.587E−7	1.040E−14	1.021E−14				Zr	4.282E−3	4.282E−3
FP[a]	1.190E−13	2.474E−3	7.581E−14	2.764E−4				FP[a]	2.708E−18	2.344E−3
O	1.721E−2	1.721E−2	1.894E−2	1.894E−2						
Fe	1.298E−2	1.298E−2	1.246E−2	1.246E−2						
Cr	3.075E−3	3.075E−3	2.951E−3	2.951E−3						
Ni	2.913E−3	2.913E−3	2.796E−3	2.796E−3						
Mo	1.724E−4	1.724E−4	1.654E−4	1.654E−4						
Ti	9.206E−5	9.206E−5	8.837E−5	8.837E−5						
Si	3.336E−4	3.336E−4	3.203E−4	3.203E−4						
Mn	3.010E−4	3.010E−4	2.889E−4	2.889E−4						
Na	7.180E−3	7.180E−3	7.162E−3	7.162E−3						

[a] Fission products.

shown in Table 20, where the final $\Delta\rho$ uncertainty is a quadratic combination of the uncertainties of actinides and fission product components.

Uncertainties are significant for K_{eff} for all systems, for the burnup reactivity swing in thermal systems (essentially due to actinides) and, to a lesser extent, for coolant void coefficients in fast systems and neutron source in thermal systems at fuel discharge. For all the other parameters, uncertainties are well within any anticipated target accuracies. It is to be noted that in the case of the decay heat at $t = 100$ years after discharge, the uncertainties are essentially due to the actinides α decay component. The values shown are due to the uncertainties of the relevant actinide uncertainties at $t = 100$ years, and a zero uncertainty was assumed for the associated decay particle energies.

The breakdown of the most significant uncertainties on integral parameters by isotope contributions (Tables 21–26), shows that the major contributors in the case of K_{eff}, are still U-238 and Pu-239. Despite the presence of significant amounts of MA in the fuel of the fast systems (in particular in the case of SFR), MA data uncertainties do not play a major role with a few exceptions (Am-241 σ_c for GFR and Am-242m σ_f for SFR).

Tables 27 and 28 give the uncertainties related to the major isotope density variations Δn during the cycle, for the GFR and VHTR respectively. Significant uncertainties are shown for the Pu-239, Am-243, Cm-244 and Pu-241 Δn values in the GFR case. The capture of U-238, Pu-240, Pu-242 and Am-243, and the fission of Pu-239 and Pu-241, play the most significant role. In the case of the VHTR, lower uncertainties on isotope density variations are observed, the largest values being related to the Δn of Np-237 (due to U-236 capture), Pu-238 (also due to the U-236 capture), Pu-240 (due to the Pu-240 capture), Am-241 (due mostly to Am-241 capture) and Am-243 (due to Pu-242 capture and Am-243 capture).

As for the energy breakdown, Table 29 is related to the GFR K_{eff} uncertainty for the major isotopes, Table 30 to the SFR and Table 31 to the VHTR K_{eff} uncertainty.

The most significant data for the different reactions/isotopes are:

- Pu-239 fission between 1 MeV and 1 keV and below 1 eV.
- Pu-239 capture below 1 eV.
- Pu-240 capture at the first resonance.

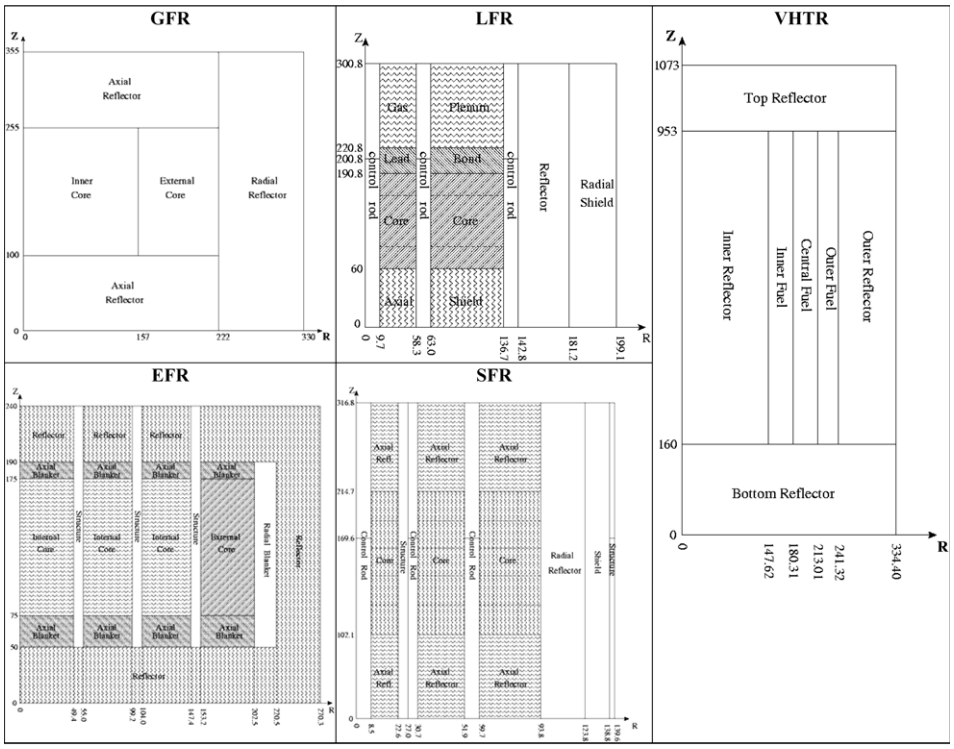

Fig. 7. Geometry details of the systems under investigation (dimensions in cm).

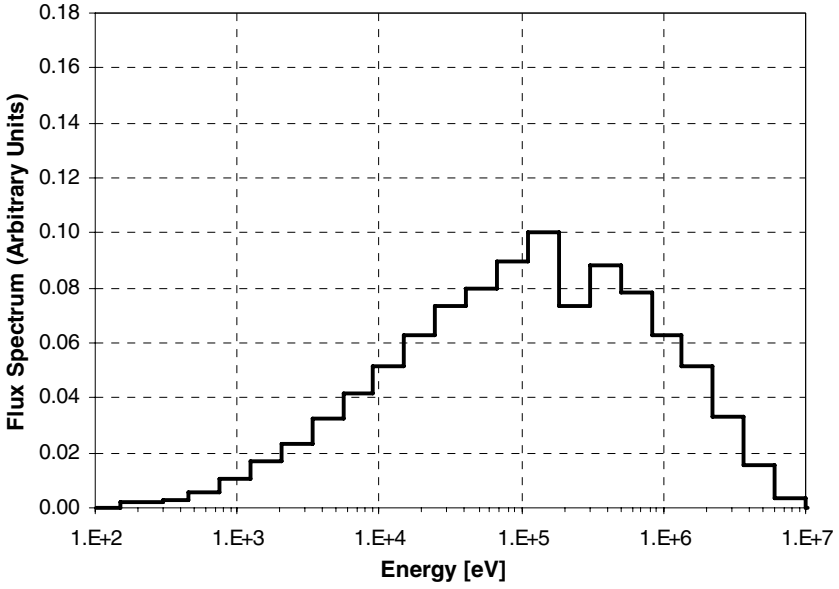

Fig. 8. GFR direct flux distribution.

- Pu-241 fission between 1 MeV and 1 keV.
- U-238 capture between 0.2 MeV and 2 keV and between 400 and 10 eV.
- Am-242m fission between 1 MeV and 10 keV.

Finally, Tables 32 and 33 give a comparison between the uncertainties that result from the use of the ANL and NEA-K covariance matrices for the GFR and VHTR systems. Comparable results are observed in the case of Pu-239 for the GFR integral parameters and of the Pu-240 for the VHTR case. In the case of U-238, Pu-241 and Si, the NEA-K covariance matrix data give lower values (factor ~2–3). This intercomparison has to be taken with precaution, since the NEA-K does not represent a fully consistent and complete set of data. However, the results seem to indicate that the present covariance evaluations would tend to show signif-

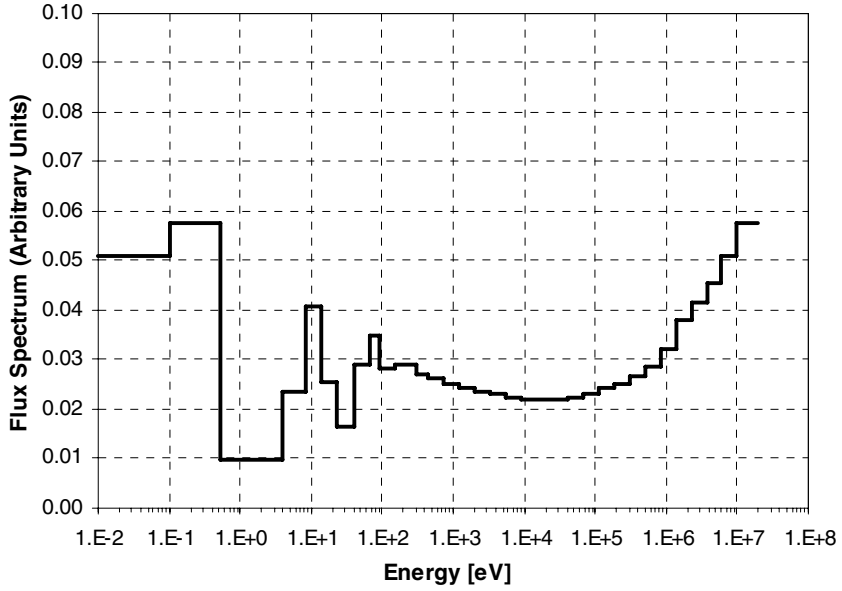

Fig. 9. GFR adjoint flux distribution.

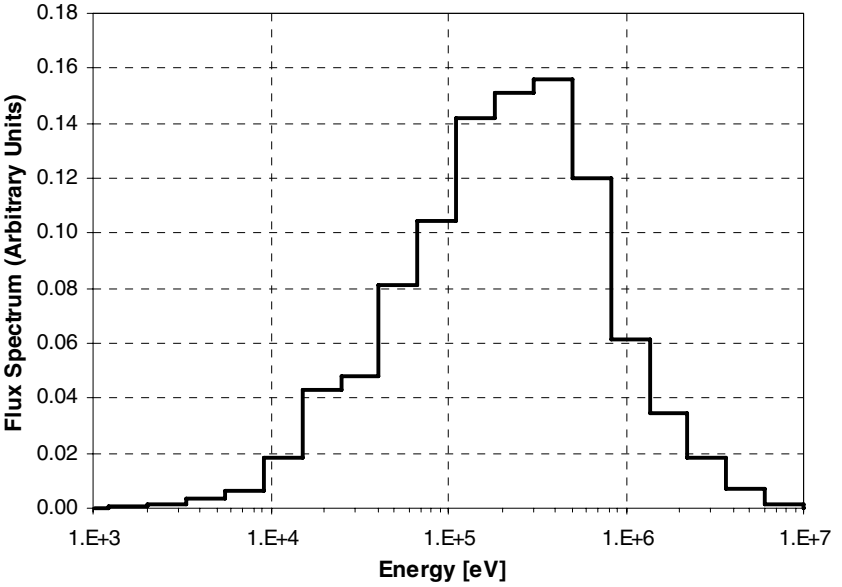

Fig. 10. LFR direct flux distribution.

icantly lower uncertainties on the integral parameters, which in principle indicate lower needs for data improvement.

5.2. Summary of lessons drawn from the uncertainty analysis

The following is a summary of the conclusions from the uncertainty analysis study. It has to be kept in mind that only neutron cross-section data have been considered in this study.

1. Data uncertainties, whatever the hypothesis, are significant only for a few parameters:
   - K_{eff} for all systems (in the case of thermal systems, at EOC due to high burnup).
   - Burnup (BU) reactivity swing and related isotope density variations Δn during core depletion.
   - Some void coefficients in fast systems.
   - To a lesser extent, neutron source (thermal systems) at fuel unloading.
   - For other parameters, the uncertainties are within anticipated target accuracies (see Section 7).
2. Despite significant MA recycling in fast systems and extended burnup in thermal systems, MA data do not play a major role. Some exceptions are:

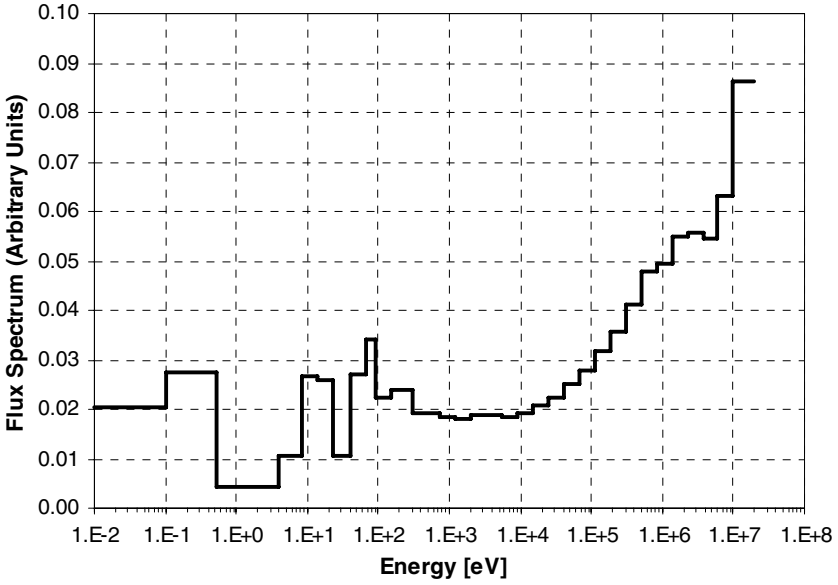

Fig. 11. LFR adjoint flux distribution.

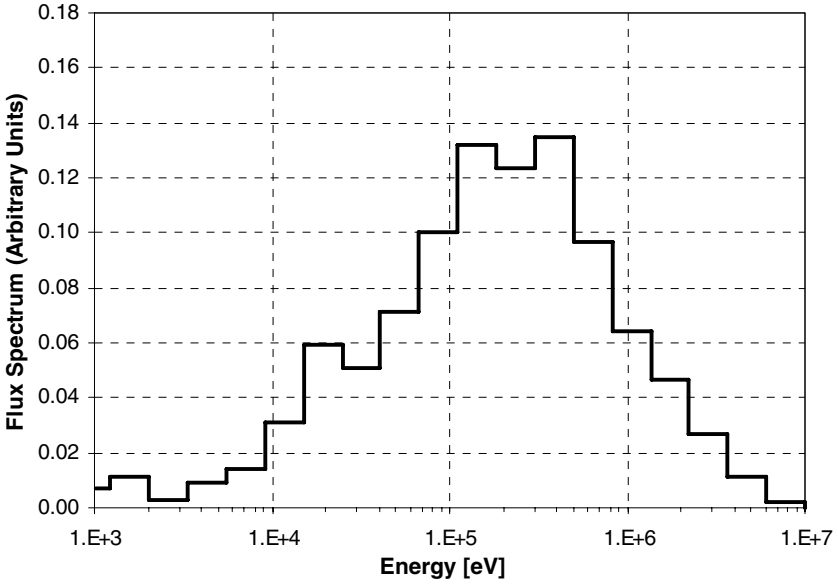

Fig. 12. SFR direct flux distribution.

- Am-241 capture in the "fast" range.
- Am-242m fission in the "fast" range.

3. For major actinides, besides U-238, Pu isotope data uncertainties are significant:
   - Pu-239 fission between 1 MeV and 1 keV and below 1 eV.
   - Pu-240 capture at the first resonance.
   - Pu-241 fission between 1 MeV and 1 keV.
   - U-238 capture between 0.2 MeV and 2 keV and between 400 and 10 eV.
   - U-238 inelastic.
4. As for structural/coolant materials, the most significant data are:
   - Fe inelastic.
   - Na elastic.
   - Pb inelastic.
   - Si inelastic.
5. These indications depend of course on the uncertainty data that have been used.
   - Consistent results have been obtained, e.g., for Pu-239 fission and Pu-240 capture (in the thermal range), when the NEA-K data (from IRDF and JENDL-3, respectively) have been used.
   - On the contrary, if JENDL-3 data are used for, e.g., Pu-241 fission and for Pu-240 in the "fast" range, or ENDF/B-VI data for Si-28, no further requirement for improvement would appear necessary. Some covariance data, in particular those for Pu-241, would require further verifications and improvements before drawing conclusions.

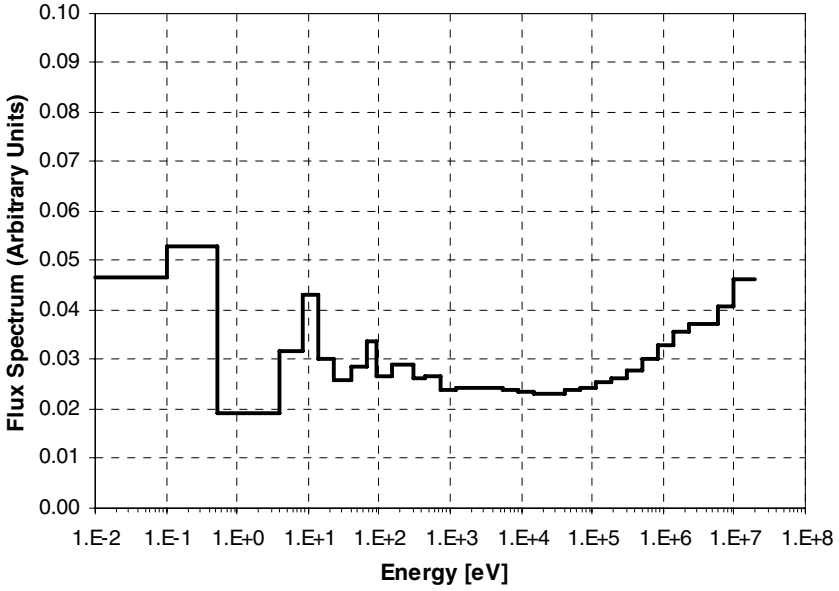

Fig. 13. SFR adjoint flux distribution.

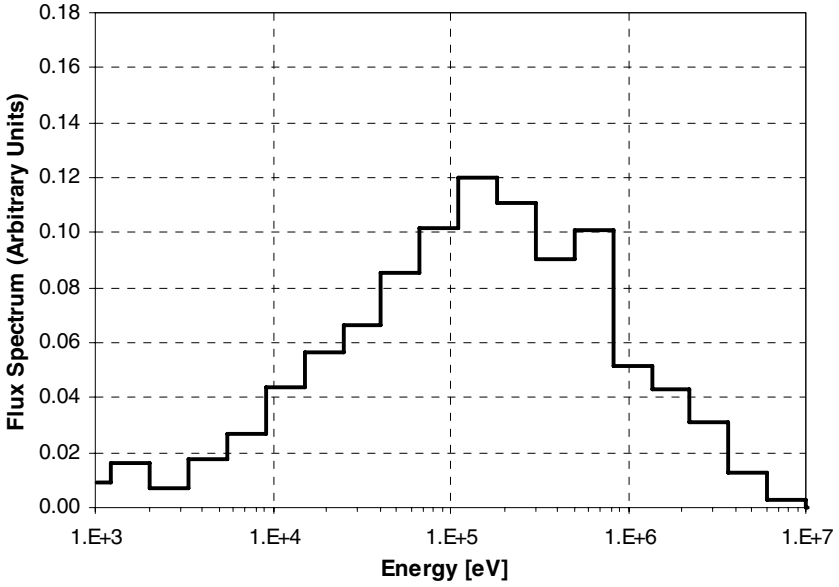

Fig. 14. EFR direct flux distribution.

Finally, we would stress that the results obtained are obviously related to the specific systems considered. The "images" we have chosen are fairly general. However, specific features can show up, when systems with less common characteristics are considered. An example will be given in the next section.

6. Uncertainty assessment of coolant void reactivity coefficient for liquid-salt-cooled VHTR

Recently, a liquid-salt (molten-salt) cooled version of the VHTR, the LS-VHTR, has been proposed to improve the system economy for the VHTR (Forsberg, 2005). The LS-VHTR would operate at a low primary system pressure using a liquid salt coolant that has better heat removal properties than the helium coolant.

One of the main issues in the design of the LS-VHTR is the coolant void reactivity coefficient. Contrary to the standard VHTR, the presence of a liquid salt can lead to a positive reactivity coefficient, in the event of a loss of coolant. In this case, the safety of the LS-VHTR can be compromised, jeopardizing the viability of the concept. We present here an analysis of the characteristics of the LS-VHTR coolant void reactivity coefficient and the implications of uncertainties in basic cross-sections on its value. The specificity of this particular VHTR design justifies a specific uncertainty analysis, since new materials and issues should be investigated.

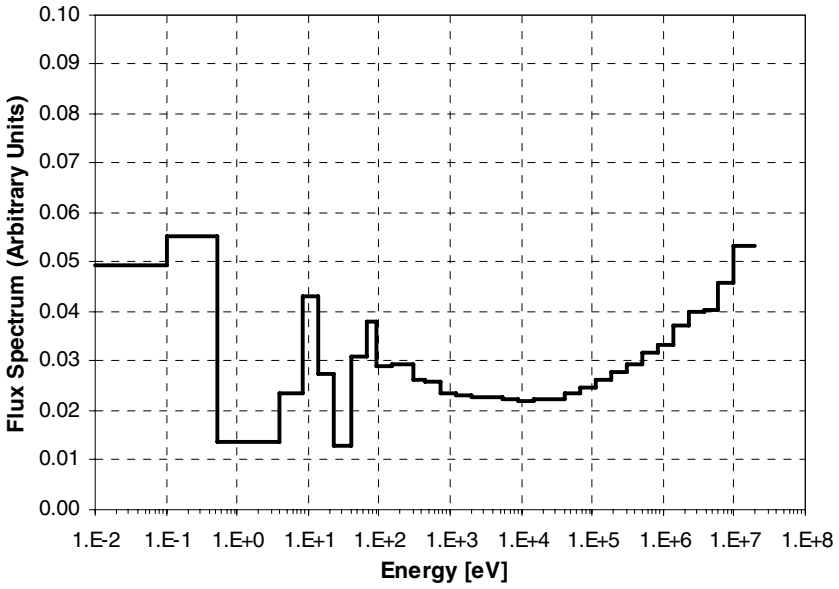

Fig. 15. EFR adjoint flux distribution.

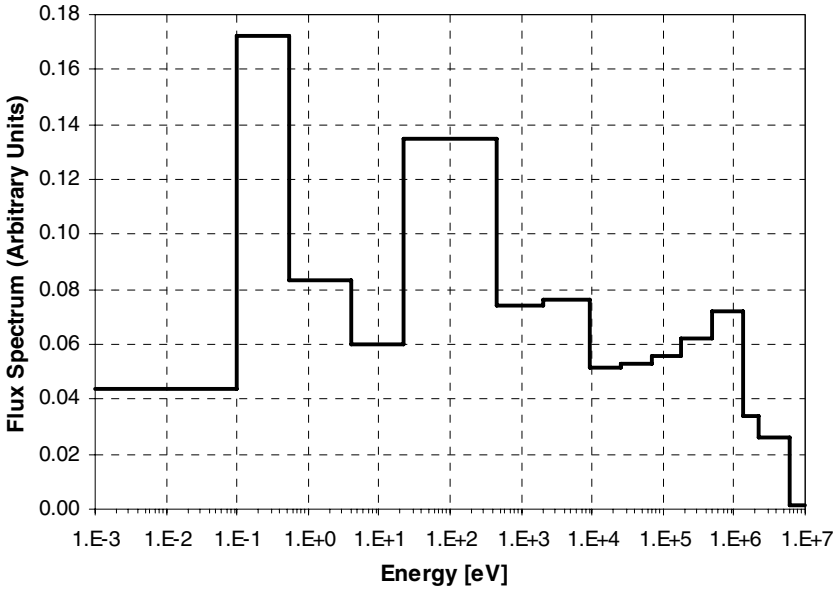

Fig. 16. VHTR direct flux distribution.

6.1. Perturbation components of coolant void reactivity coefficient

The coolant void reactivity coefficient has been calculated using an assembly model of a preliminary LS-VHTR design. The LS-VHTR fuel is contained in coated fuel particles (TRISO) which are dispersed in graphite compacts. The fuel kernel diameter is 425 μm and the packing fraction is 25%. Li_2BeF_4 has been considered a reference liquid salt coolant and the Li-7 content in Li (Li enrichment) is assumed to be 99.995%.

Table 34 provides the perturbation components of the coolant void reactivity coefficient by reactions, energy range, and isotope. The total coolant void reactivity coefficient is small but of positive sign (22 pcm). The small value is the result of compensation between the capture component, which is positive, and the scattering one that is negative. The capture component has the largest values in the thermal energy range containing the flux spectrum peak. The negative capture value in group 2 is due to the $(n, 2n)$ Be cross-section (included in the capture cross-section) that generates neutrons instead of absorption.

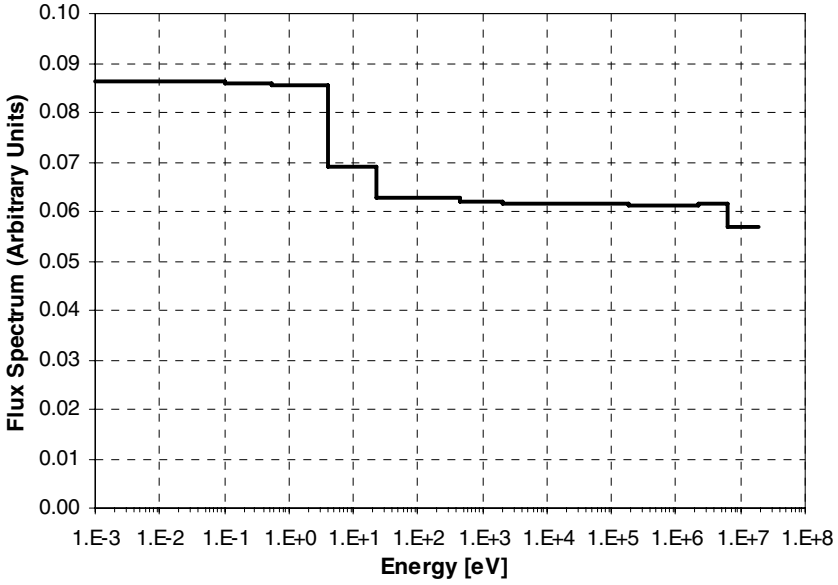

Fig. 17. VHTR adjoint flux distribution.

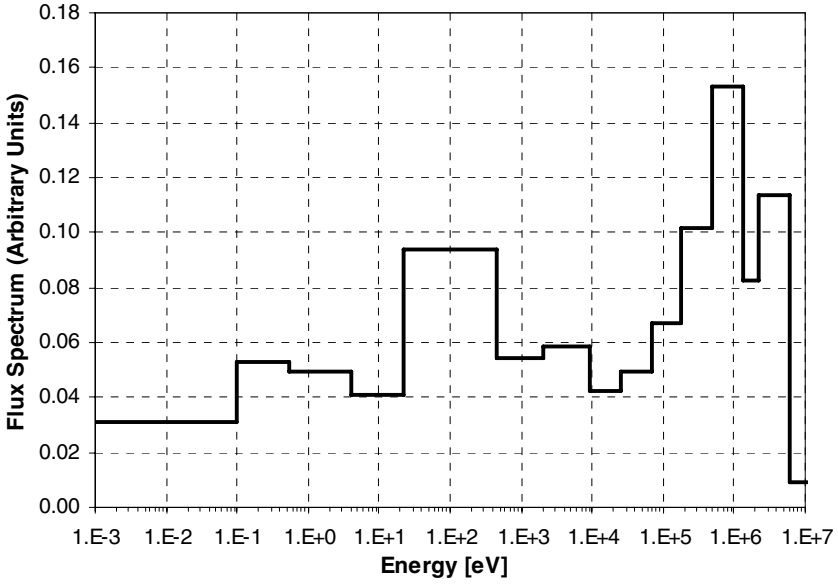

Fig. 18. PWR direct flux distribution.

The scattering component has the largest values in groups 11 and 12. This is due to the slowing down of neutrons toward a region of spectrum with increased neutron importance. The fission component, though small when compared to the capture and scattering components, still gives a significant negative contribution to the total value. Regarding the contribution by isotope, the U-238 and Li-6 give large positive contributions due to their capture cross-sections, while Be and F give negative contributions. The total value for F is the result of competition between capture and scattering components that ends up in a negative contribution. The same competition produces a positive value for Li-7.

6.2. Uncertainty evaluation

Table 35 shows the uncertainty evaluation for the coolant void reactivity coefficient of the LS-VHTR based on the sensitivity analysis by Kim et al. (2005). Results have been obtained using the ANL covariance matrix (Palmiotti and Salvatores, 2005), and sums are statistical ones (square root of sum of squares) with no correlations among the different cross-sections.

One first observation is that the total uncertainty is greater than 100%, indicating that with the adopted cross-section uncertainties the sign of the coolant void

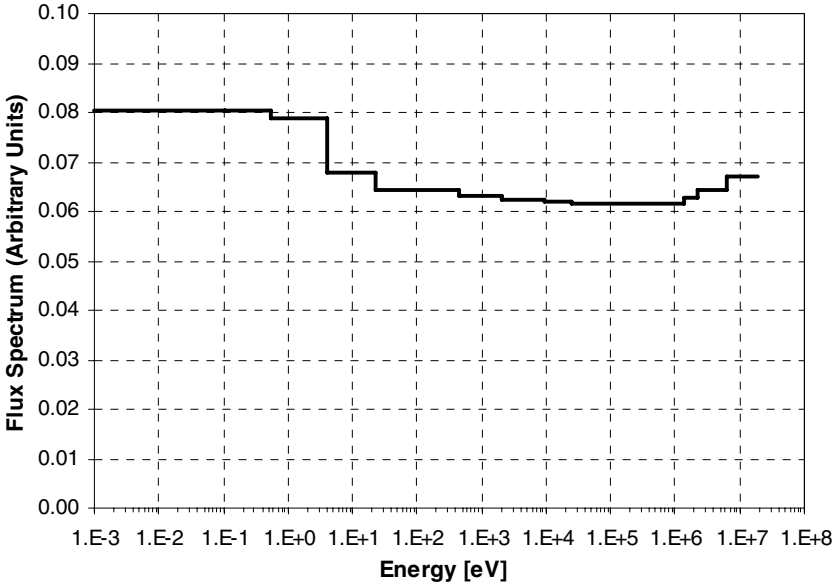

Fig. 19. PWR adjoint flux distribution.

Table 13
GFR, LFR, SFR, and EFR nominal values

Reactor	Reactivity (pcm)	Power peak	Temperature reactivity coefficient (pcm)	Void reactivity coefficient (pcm)	Burnup reactivity $\Delta\rho$ (pcm)
GFR	1038.0	1.45[a]	1549[b]	350.1[c]	1081.3[d]
LFR	22.9	1.29[e]	228.1[f]	6575.5[g]	−1464[h]
SFR	5015.4	1.53[i]	231[l]	1831[m]	−3981.1[n]
EFR	9786.5	1.63[o]	1289[p]	1934.5[q]	−9123.9[r]

[a] Center core radially and axially.
[b] $\rho\ (T_{core} = 300\ K) - \rho(T_{core} = 1263\ K)$.
[c] He loss in core and reflector.
[d] 415 days irradiation.
[e] $(R, Z) = (100.96, 117.90)_{cm}$.
[f] $\rho(T_{core} = 300\ K) - \rho(T_{core} = 900\ K)$.
[g] Pb loss in core.
[h] 310 days irradiation.
[i] $(R, Z) = (66.59, 143.03)_{cm}$.
[l] $\rho(T_{core} = 300\ K) - \rho(T_{core} = 850\ K)$.
[m] Na loss in core.
[n] 155 days irradiation.
[o] $(R, Z) = (153.24, 125)_{cm}$.
[p] $\rho(T_{core} = 300\ K) - \rho(T_{core} = 1520\ K)$.
[q] Na loss in core and blanket.
[r] 1700 days irradiation.

reactivity effect cannot be ensured. On the other hand, one can argue that in view of the very small coefficient value (+22 pcm) this result could have been expected, while in the case of a larger nominal value the total uncertainty should be smaller, because this is a relative variation. The large values at high energy are due to the graphite scattering cross-section, that has an uncertainty of 30% in the covariance matrix. Groups 11 and 12 are dominated by the contribution of scatterers like graphite (3% uncertainty in the covariance matrix), Be, F and Li-7,

Table 15
PWR nominal values

K_{eff}[a]	K_{eff}[b]	Temperature[c] reactivity coefficient (pcm)	Temperature[d] reactivity coefficient (pcm)	Burnup[e] reactivity $\Delta\rho$ (pcm)
1.49802	0.87231	695.2	1054.6	−47883.6

[a] BOC.
[b] EOC.
[c] $\rho(T_{core} = 550\ K) - \rho(T_{core} = 900\ K)$ at BOC.
[d] $\rho(T_{core} = 550\ K) - \rho(T_{core} = 900\ K)$ at EOC.
[e] 2773.5 days.

Table 14
VHTR nominal values

K_{eff}[a]	K_{eff}[b]	Peak power[c]	Peak power[d]	Temperature[e] reactivity coefficient (pcm)	Temperature[f] reactivity coefficient (pcm)	Burnup[g] reactivity $\Delta\rho$ (pcm)
1.37767	1.01610	1.96	2.25	2095.3	3416.3	−25829.4

[a] BOC.
[b] EOC.
[c] BOC at $(R, Z) = (147.62, 556.5)_{cm}$.
[d] EOC at $(R, Z) = (147.62, 556.5)_{cm}$.
[e] $\rho(T_{core} = 773\ K) - \rho(T_{fuel} = 1373\ K;\ T_{moderator} = 1200\ K)$ at BOC.
[f] $\rho(T_{core} = 773\ K) - \rho(T_{fuel} = 1373\ K;\ T_{moderator} = 1200\ K)$ at EOC.
[g] 845.63 days irradiation.

Table 16
Fast neutron systems – total uncertainties (%)

Reactor		K_{eff}	Power peak	Temperature reactivity coefficient	Void reactivity coefficient	Burnup $\Delta\rho$ (pcm)	Decay heat	Dose	Neutron source
GFR	NC[a]	±1.20	±1.2	±3.6	±4.8	±240	±0.3	±0.4	±1.2
	PEC[b]	1.90	1.8	5.5	7.1	384	0.5	0.6	1.8
LFR	NC	1.51	0.8	5.2	13.0	177	0.3	0.4	0.8
	PEC	2.26	1.0	7.8	20.6	258	0.6	0.5	1.2
SFR	NC	1.10	0.4	4.1	17.8	156	0.2	0.2	0.6
	PEC	1.66	0.5	6.0	23.4	234	0.4	0.2	0.9
EFR	NC	1.02	0.7	3.4	8.4	652	1.6	1.1	3.9
	PEC	1.57	1.1	5.1	12.1	989	2.3	1.7	6.0

[a] NC, no correlation.
[b] PEC, partial energy correlation.

Table 17
VHTR total uncertainties (%)

	K_{eff}		Peak power		Temperature reactivity coefficient		Burnup $\Delta\rho$ (pcm)	Decay heat	Dose	Neutron source
	BOC	EOC	BOC	EOC	BOC	EOC				
NC[a]	±0.41	±0.94	±0.87	±0.93	±3.6	±5.8	±1482	±2.5	±1.9	±12.2
PEC[b]	0.58	1.07	1.0	1.1	3.3	5.5	1574	3.1	2.6	14.3

[a] NC, no correlation.
[b] PEC, partial energy correlation.

Table 18
Extended burnup PWR total uncertainties (%)

	K_{eff}		Temperature reactivity coefficient		Burnup $\Delta\rho$ (pcm)	Decay heat	Dose	Neutron source
	BOC	EOC	BOC	EOC				
NC[a]	±0.33	±0.97	±2.1	±4.0	±1916	±2.9	±2.3	±11.2
PEC[b]	0.52	1.27	3.1	4.6	2206	3.8	3.1	13.3

[a] NC, no correlation.
[b] PEC, partial energy correlation.

Table 19
$\Delta\rho$ burnup breakdown into components (pcm)

System	GFR	LFR	SFR	EFR	VHTR	PWR
$\Delta\rho$ component						
Actinides	2142	−886	−3390	−2798	−14,754	−35,674
Fission products						
Capture component	−844	−390	−452	−5098	−10,753	−12,205
Scattering component (elastic + inelastic)	−230	−185	−140	−1228	−378	–
Total	1068	−1461	−3982	−9124	−25,885	−47,879

all with 7% uncertainty for the scattering cross-section in these groups. In the same energy groups the 5% uncertainty on U-238 capture leads to significant contributions. At thermal energies, groups 14 and 15, the large uncertainty values are determined by the contribution of Li-6 and Li-7 capture cross-sections that have a 5% uncertainty value.

A target accuracy assessment, as discussed in the following section, would be very helpful in determining the uncertainty levels to which specific cross-sections have to be

Table 20
$\Delta\rho$ burnup uncertainty breakdown into components (pcm)

System	GFR	LFR	SFR	EFR	VHTR	PWR
$\Delta\rho$ component						
Actinides	±340	±258	±234	±989	±1574	±2206
Fission products	±130	±76	±73	±755	±215	±244
Total	±364	±269	±245	±1244	±1589	±2219

Table 21
GFR uncertainties (%) PEC – breakdown by isotope (major contributions)

Isotope	K_{eff}	Temperature reactivity coefficient (BOC)	Void reactivity coefficient (BOC)	Burnup $\Delta\rho$ (pcm)
U-238	±1.22	±3.2	±3.9	±63
Pu-238	0.22	0.6	0.7	85
Pu-239	1.03	2.6	2.6	203
Pu-240	0.29	0.7	0.7	14
Pu-241	0.57	1.5	1.7	189
Am-241	0.43	1.8	1.2	73
Am-242m	0.01	0.0	0.0	76
Cm-242	0.00	0.0	0.0	90
Cm-244	0.13	0.4	0.3	35
Cm-245	0.17	0.4	0.5	38
C	0.31	1.9	1.7	8
Si-28	0.42	1.2	0.7	12
Zr-90	0.12	0.3	0.5	9

Table 22
LFR uncertainties (%) PEC – breakdown by isotope (major contributions)

Isotope	K_{eff}	Temperature reactivity coefficient (BOC)	Void reactivity coefficient (BOC)	Burnup $\Delta\rho$ (pcm)
U-238	±0.73	±2.2	±3.7	±13
Pu-238	0.24	0.5	0.9	25
Pu-239	1.50	3.4	4.0	213
Pu-240	0.41	1.1	0.9	18
Pu-241	0.32	0.7	1.0	112
Am-241	0.10	0.4	0.3	6
Am-242m	0.06	0.1	0.2	14
Cm-242	0.02	0.0	0.0	11
Cm-244	0.13	0.3	0.2	12
Cm-245	0.21	0.4	0.7	34
Fe-56	0.24	1.6	2.0	5
Pb-206	0.88	3.2	13.4	18
Pb-207	0.80	3.4	12.2	16
Pb-208	0.49	4.0	7.4	8

lowered in order to achieve a more reasonable value (e.g., 20%) for the uncertainty on the LS-VHTR coolant void reactivity coefficient.

The example of this section underlines that a generic analysis, as performed in this paper, has to be complemented with specific studies, if the analysis is required of a specific variant of one of the selected concepts.

Table 23
SFR uncertainties (%) PEC – breakdown by isotope (major contributions)

Isotope	K_{eff}	Temperature reactivity coefficient (BOC)	Void reactivity coefficient (BOC)	Burnup $\Delta\rho$ (pcm)
U-238	±0.21	±0.8	±1.9	±15
Pu-238	0.34	1.1	3.8	53
Pu-239	0.88	2.5	5.5	99
Pu-240	0.52	1.3	4.4	45
Pu-241	0.51	1.7	4.3	109
Pu-242	0.23	0.6	1.6	21
Am-241	0.13	0.8	1.2	7
Am-242m	0.64	1.9	4.1	89
Cm-242	0.04	0.1	0.3	15
Cm-244	0.36	1.1	2.8	58
Cm-245	0.37	1.2	3.0	64
Fe-56	0.62	2.9	8.3	45
Na-23	0.34	2.4	18.7	30

Table 24
EFR uncertainties (%) PEC – breakdown by isotope (major contributions)

Isotope	K_{eff}	Temperature reactivity coefficient (BOC)	Void reactivity coefficient (BOC)	Burnup $\Delta\rho$ (pcm)
U-238	±0.78	±2.2	±2.7	±104
Pu-238	0.10	0.4	0.8	64
Pu-239	1.23	3.9	3.9	775
Pu-240	0.35	1.2	1.6	91
Pu-241	0.21	0.7	1.3	485
Am-241	0.07	0.4	0.4	37
Am-242m	0.02	0.1	0.1	28
Cm-242	0.00	0.0	0.0	22
Cm-244	0.05	0.2	0.2	47
Cm-245	0.06	0.2	0.3	66
Fe-56	0.26	0.9	1.2	68
Na-23	0.22	1.3	10.8	63
O-16	0.14	1.2	0.6	61

Table 25
VHTR uncertainties (%) PEC – breakdown by isotope (major contributions)

Isotope	K_{eff}		Temperature reactivity coefficient		Burnup $\Delta\rho$ (pcm)	Neutron source
	BOC	EOC	BOC	EOC		
U-235	±0.36	±0.25	±1.3	±0.6	±171	±0.02
U-238	0.43	0.55	2.7	2.2	150	2.61
Pu-239	0.00	0.57	0.0	3.0	624	2.26
Pu-240	0.00	0.63	0.0	3.9	1313	2.60
Pu-241	0.00	0.17	0.0	0.3	222	2.33
Pu-242	0.00	0.02	0.0	0.1	36	3.95
Am-243	0.00	0.02	0.0	0.1	27	12.60
Cm-244	0.00	0.00	0.0	0.0	3	2.30

7. Target accuracy

As a general feature, the integral parameter uncertainties resulting from the assumed uncertainties on nuclear

Table 26
Extended burnup PWR uncertainties (%) PEC – breakdown by isotope (major contributions)

Isotope	K_{eff}		Temperature reactivity coefficient		Burnup $\Delta\rho$ (pcm)	Neutron source
	BOC	EOC	BOC	EOC		
U-235	±0.35	±0.16	±1.0	±0.3	±228	±0.02
U-238	0.36	0.69	2.8	3.2	391	2.19
Pu-239	0.00	0.62	0.0	1.7	637	2.07
Pu-240	0.00	0.62	0.0	2.4	1727	2.45
Pu-241	0.00	0.32	0.0	0.2	359	2.38
Pu-242	0.00	0.07	0.0	0.0	111	3.49
Am-243	0.00	0.14	0.0	0.1	197	10.01
Cm-244	0.00	0.06	0.0	0.0	78	6.48

data, as summarized in Tables 16–18, are quite acceptable both in the phase of design feasibility studies and in the subsequent phase of preliminary conceptual design. In fact, the uncertainties shown in Tables 16–18, will not prevent performing meaningful parametric and optimization studies, nor evaluating, on a comparative basis, the impact of technological choices. This consideration is valid both for the reactor design and for the assessment of the major physics parameters of the associated fuel cycles.

The state-of-the-art is obviously dependent on the assumed uncertainties and covariance data associated with the present nuclear data files, in particular ENDF/B and JEFF latest versions. We recall here that, despite some rather arbitrary assumptions, the creation of the ANL covariance data did consider the performance of the nuclear data files in the prediction of selected, high precision integral measurements.

No major short term need, in terms of reduction of unacceptably high nuclear data uncertainties is evident from the present work.

However, later design phases of selected reactor and fuel cycle concepts, will need improved data and methods, in order to reduce margins, both for economical and safety reasons. At that stage, it will be relevant to define priority issues, i.e. which are the nuclear data (isotope, reaction type, and energy range) that need improvement, to quantify target accuracies and to select a strategy to meet the requirement, e.g. by new differential measurements or by the use of integral experiments. In this respect one should account for the wide range of high accuracy integral

Table 27
GFR: uncertainties (%) on the $\Delta n = n_{t_F} - n_0$ isotope concentration variation during irradiation

		Pu-239	Pu-241	Am-241	Am-243	Cm-244
U-238	Capture	±15.62				
	Fission	0.05				
	n, 2*n*	0.01				
Pu-239	Capture	5.44	0.14			
	Fission	9.37	0.00			
	n, 2*n*	0.06	0.00			
Pu-240	Capture		7.92	0.09		
	Fission		0.05	0.00		
	n, 2*n*		0.00	0.00		
Pu-241	Capture		2.40	0.03		
	Fission		6.90	0.08		
	n, 2*n*		0.13	0.00		
Pu-242	Capture				10.10	0.38
	Fission				0.13	0.00
	n, 2*n*				0.00	0.00
Am-241	Capture			5.85	0.25	
	Fission			1.38	0.00	
	n, 2*n*			0.00	0.00	
Am-243	Capture				14.21	9.10
	Fission				2.90	0.11
	n, 2*n*				0.00	0.00
Cm-244	Capture					4.16
	Fission					4.90
	n, 2*n*					0.02
PEC		19.03	10.78	6.01	17.69	11.15

PEC case.

Table 28
VHTR: uncertainties (%) on the $\Delta n = n_{t_F} - n_0$ isotope concentration variation during irradiation

		Np-237	Pu-238	Pu-239	Pu-240	Pu-241	Pu-242	Am-241	Am-243
U-235	Capture	±1.45	±1.31	±0.00	±0.00				
U-236	Capture	6.97	6.31	0.02	0.01				
U-238	Capture	0.00	0.28	2.52	2.55	2.58	2.62	2.60	2.63
Np-237	Capture	1.40	2.75	0.01	0.01				
Pu-238	Capture		1.26	0.02	0.01				
Pu-239	Capture		0.23	1.02	1.83	1.91	2.05	1.98	2.13
	Fission		0.07	1.07	1.02	0.94	0.80	0.86	0.72
Pu-240	Capture		0.26		5.73	0.94	1.76	1.38	2.26
Pu-241	Capture		0.04			0.56	2.34	0.50	2.39
	Fission		0.08			1.10	0.88	0.98	0.76
Pu-242	Capture						1.02		4.12
Am-241	Capture		0.43				0.03	5.50	0.06
Am-243	Capture								4.62
PEC		7.26	7.15	2.92	6.61	3.69	4.70	6.69	7.85

PEC case.

Table 29
GFR BOC K_{eff} uncertainties

Gr.	Energy[a]	U-238σ_{capt}	U-238σ_{in}	Pu-239σ_{fiss}	Pu-241σ_{fiss}	Am-241σ_{capt}	Si-28σ_{in}
1	19.6 MeV	±0	±36	±9	±5	±0	±26
2	6.07 MeV	8	524	90	54	0	292
3	2.23 MeV	14	292	92	30	1	93
4	1.35 MeV	61	151	236	76	23	0
5	498 keV	61	18	243	96	43	0
6	183 keV	97	21	289	139	74	0
7	67.4 keV	157	1	240	140	79	0
8	24.8 keV	180	0	201	134	76	0
9	9.12 keV	134	0	255	184	107	0
10	2.03 keV	77	0	106	116	84	0
11	454 eV	19	0	38	41	33	0
12	22.6 eV	0	0	1	1	1	0
13	4.00 eV	0	0	0	0	0	0
14	0.54 eV	0	0	0	0	0	0
15	0.10 eV	0	0	0	0	0	0
Total (pcm)		314	620	625	353	199	307

Energy breakdown (pcm).
[a] Upper bound.

Table 30
SFR K_{eff} BOC uncertainties

Gr.	Energy[a]	Pu-238σ_{fiss}	Pu-239σ_{fiss}	Pu-240σ_{fiss}	Pu-241σ_{fiss}	Am-242mσ_{fiss}	Cm-244σ_{fiss}	Fe-56σ_{in}	Na-23σ_{in}
1	19.6 MeV	±4	±7	±9	±6	±3	±8	±30	±9
2	6.07 MeV	36	76	81	59	39	75	111	51
3	2.23 MeV	40	87	89	37	38	75	114	42
4	1.35 MeV	113	261	185	109	138	189	242	238
5	498 keV	94	351	42	180	262	33	0	1
6	183 keV	50	293	18	183	258	9	0	0
7	67.4 keV	90	148	10	111	152	5	0	0
8	24.8 keV	80	118	6	101	70	4	0	0
9	9.12 keV	35	43	3	43	29	1	0	0
10	2.03 keV	64	44	8	65	47	2	0	0
11	454 eV	11	13	0	17	11	0	0	0
12	22.6 eV	0	1	0	3	1	0	0	0
13	4.00 eV	0	0	0	0	1	0	0	0
14	0.54 eV	0	0	0	0	0	0	0	0
15	0.10 eV	0	0	0	0	0	0	0	0
Total (pcm)		217	575	227	334	434	220	291	247

Energy breakdown (pcm).
[a] Upper bound.

experiments already performed and available in national or, better, international data basis.

To provide a first indicative answer to the questions raised above, we have applied the methodology described in Section 2.1, and attempted a first target accuracy assessment.

Regarding target accuracies on integral parameters, we have defined a tentative first set for the multiplication factor, K_{eff}, the power peak, the temperature and coolant void reactivity coefficients, the reactivity loss during irradiation and the transmutation potential (i.e., nuclide concentrations at end of irradiation). The target accuracies have been fixed as shown in Table 36. For nuclear fuel cycle related parameters (i.e., decay heat, neutron source, and dose) we considered a target accuracy of 20%. These values are of course rather arbitrary, but are consistent with standard requirements for reactor design in early phases of development. It can be observed that the peak power, the reactivity coefficient, and the nuclear fuel cycle related parameters as shown in Tables 16–18 meet the accuracy requirements in all cases.

We have used the formulation shown in Section 2.1, with the sensitivity coefficients obtained from GPT calculations and assuming that the "cost" parameters λ are set equal to 1. To avoid the introduction of meaningless parameters, we have chosen as unknown "*d*" parameters (i.e., as cross-sections for which target accuracies are required), only those which globally account at least for

Table 31
VHTR EOC K_{eff} uncertainties (pcm)

Gr.	Energy[a]	U-235σ_{fiss}	U-238σ_{capt}	Pu-239σ_{capt}	Pu-239σ_{fiss}	Pu-240σ_{capt}	Pu-241σ_{fiss}
1	19.6 MeV	±0	±0	±0	±0	±0	±0
2	6.07 MeV	1	0	0	0	0	1
3	2.23 MeV	1	0	0	1	0	0
4	1.35 MeV	2	2	0	1	0	1
5	498 keV	2	2	0	1	0	1
6	183 keV	2	2	0	1	0	1
7	67.4 keV	2	4	0	1	0	1
8	24.8 keV	3	7	0	1	0	1
9	9.12 keV	8	10	1	1	0	2
10	2.03 keV	10	24	1	2	1	4
11	454 eV	51	185	11	13	11	26
12	22.6 eV	34	337	11	15	2	56
13	4.00 eV	38	8	5	12	620	6
14	0.54 eV	80	9	360	346	24	88
15	0.10 eV	46	5	21	23	6	23
Total (pcm)		118	385	361	347	621	110

[a] Upper bound.

Table 32
GFR comparison of results with the covariance matrix by Palmiotti and Salvatores (2005) with partial energy correlation (PEC), and NEA-K covariance matrix

		K_{eff}	Temperature reactivity coefficient (BOC)	Void reactivity coefficient (BOC)	Burnup $\Delta\rho$ (pcm)
U-238	PEC	±1.22	±3.2	±3.9	±63
	NEA-K	0.58	1.6	1.5	31
Pu-239	PEC	1.03	2.6	2.6	203
	NEA-K	1.20	2.4	3.3	160
Pu-240	PEC	0.29	0.7	0.7	14
	NEA-K	0.08	0.2	0.1	5
Pu-241	PEC	0.57	1.5	1.7	189
	NEA-K[a]	(0.11)	(0.1)	(0.3)	(39)
Si	PEC	0.42	1.2	0.7	12
	NEA-K	0.09	0.4	0.3	3
Zr	PEC	0.12	0.3	0.5	9
	NEA-K	0.02	0.1	0.0	1

[a] Covariance matrices appear to be underestimated and/or incomplete.

Table 33
VHTR comparison of results with the covariance matrix by Palmiotti and Salvatores (2005) with partial energy correlation (PEC), and NEA-K covariance matrix

		K_{eff} (BOC)	K_{eff} (EOC)	Burnup $\Delta\rho$ (pcm)
U-238	PEC	±0.43	±0.55	±150
	NEA-K	0.19	0.24	60
Pu-239	PEC	0.00	0.57	624
	NEA-K	0.00	0.18	211
Pu-240	PEC	0.00	0.63	1313
	NEA-K	0.00	0.51	1017
Pu-241	PEC	0.00	0.17	222
	NEA-K[a]	0.00	(0.05)	(73)

[a] Covariance matrices appear to be underestimated and/or incomplete.

Table 34
LS-VHTR coolant void reactivity coefficient perturbation components (pcm)

Gr.	Upper energy (MeV)	Capture	Fission	Scattering	Total
1	19.6	3.1	−0.1	−12.6	−9.6
2	6.07	−25.9	−0.8	8.8	−17.9
3	2.23	19.8	−0.5	3.0	22.3
4	1.35	2.7	−0.2	0.2	2.8
5	4.98e−1	2.9	−0.1	−0.9	1.9
6	1.83e−1	6.2	0.1	−2.2	4.0
7	6.74e−2	46.6	0.0	−5.9	40.7
8	2.48e−2	10.6	0.1	−4.2	6.4
9	9.12e−3	1.3	0.0	−9.5	−8.2
10	2.04e−3	2.5	0.0	−24.8	−22.3
11	4.54e−4	43.0	−0.8	−245.6	−203.4
12	2.26e−5	82.2	1.2	−509.1	−425.7
13	4.00e−6	78.0	5.5	−13.1	70.3
14	5.40e−7	436.3	−46.2	−39.7	350.4
15	1.00e−7	210.8	−4.4	4.1	210.5
Total		920.0	−46.3	−851.4	22.3

Isotope	Capture	Fission	Scattering	Total
U-235	39.5	−45.3	0.0	−5.8
U-238	104.8	−1.0	0.0	103.8
Si	1.2	0.0	−0.1	1.2
C	4.4	0.0	−50.3	−45.9
Li-6	339.7	0.0	0.0	339.7
Li-7	224.4	0.0	−127.5	96.9
Be	−63.2	0.0	−289.1	−352.4
F	269.2	0.0	−384.2	−115.0
Total	920.0	−46.3	−851.4	22.3

95% of the overall uncertainty for each integral parameter.

The cross-sections uncertainties required for satisfying the target accuracies are then calculated by a minimization

Table 35
LS-VHTR void reactivity coefficient uncertainties (%)

Gr.	Upper energy (MeV)	Capture	Fission	ν	Scattering	Total
1	19.6	13.3	0.2	0.1	26.7	29.8
2	6.07	46.1	1.0	0.8	17.9	49.5
3	2.23	7.7	0.9	0.8	6.0	9.8
4	1.35	1.0	0.8	0.4	0.7	1.5
5	4.98e−1	1.6	1.1	0.6	0.8	2.2
6	1.83e−1	2.2	0.7	0.4	1.8	2.9
7	6.74e−2	15.5	0.6	0.3	4.5	16.2
8	2.48e−2	3.7	0.5	0.3	0.7	3.8
9	9.12e−3	1.6	1.2	0.6	2.5	3.2
10	2.04e−3	3.7	1.5	0.6	6.6	7.7
11	4.54e−4	25.2	7.9	3.4	57.9	63.7
12	2.26e−5	36.5	3.1	2.0	75.9	84.2
13	4.00e−6	16.2	1.3	4.9	2.1	17.1
14	5.40e−7	51.8	10.0	8.5	1.1	53.5
15	1.00e−7	30.3	17.9	16.1	0.4	38.6
Total		92.0	22.4	19.3	101.3	140.0
Isotope		Capture	Fission	ν	Scattering	Total
U-235		17.8	22.3	19.3	0.0	34.5
U-238		41.8	1.2	1.1	0.2	41.9
Si		6.0	0.0	0.0	0.4	6.1
C		11.1	0.0	0.0	87.6	88.3
Li-6		48.7	0.0	0.0	0.0	48.7
Li-7		32.2	0.0	0.0	13.8	35.0
Be		38.8	0.0	0.0	29.2	48.5
F		36.3	0.0	0.0	39.2	53.5
Total		92.0	22.4	19.3	101.3	140.0

Table 36
Target accuracies assumed for integral parameters

	K_{eff}	Power peak	Temperature reactivity coefficient	Void reactivity coefficient	Burnup $\Delta\rho$	Transmutation
Target accuracy	±0.5%	±3%	±10%	±10%	300 pcm (fast reactors) 500 pcm (thermal reactors)	±5%

process as implemented in the SNOPT code (Gill et al., 1997) that solves optimization problems with nonlinear objective function and nonlinear constraints. SNOPT uses a sequential quadratic programming (SQP) algorithm that obtains search directions from a sequence of quadratic programming subproblems. Each QP subproblem minimizes a quadratic model of a certain Lagrangian function subject to a linearization of the constraints. An augmented Lagrangian merit function is reduced along each search direction to ensure convergence from any starting point.

The selected parameters are shown in Tables 37–42, together with the initial uncertainty and the new required uncertainty, as a result of the minimization procedure outlined in Section 2.1. In Tables 43–46, for each system under study we show:

(a) the initial uncertainties on the integral parameters;
(b) the uncertainties resulting from the new required uncertainties on data;

The required accuracy are not completely met because of the cross-sections not accounted in the minimization procedures which give as a consequence a residual uncertainty which should be added to the specified accuracy.

Despite this fact, the results are very encouraging, since most of the integral parameters uncertainties can be brought within the target accuracy. However, from the results of Tables 37–42 one can observe that in many cases very stringent requirements have been obtained (e. g. Pu-240 for the VHTR case, U-238 inelastic for GFR, etc.), which will be difficult to achieve even with very sophisticated measurement techniques or/and evaluations.

In view of the stringent requirements that have been obtained there is a strong indication that integral experiments and statistical data adjustments (Cecchini et al., 1964) will likely continue in the future to play a role in assessing the good quality of nuclear data and providing "ad hoc" solutions for reduced margin neutronics designs.

Table 37
Results of the target accuracy study for the GFR reactor

Isotope	Cross-section	Energy range	Uncertainty		Isotope	Cross-section	Energy range	Uncertainty		Isotope	Cross-section	Energy range	Uncertainty	
			Initial	Required				Initial	Required				Initial	Required
U-238	σ_{capt}	1.35 MeV–498 keV	5	3.9	Pu-240	σ_{capt}	183–67.4 keV	20	8.7	Cm-243	σ_{fiss}	183–67.4 keV	40	26.9
		498–183 keV	5	3.9			67.4–24.8 keV	20	7.4			67.4–24.8 keV	40	26.9
		183–67.4 keV	5	3.1			9.12–2.03 keV	10	6.4			9.12–2.03 keV	40	26.9
		67.4–24.8 keV	5	2.5			2.03 keV–454 eV	10	6.7	Cm-244	σ_{fiss}	1.35 MeV–498 keV	40	11.6
		24.8–9.12 keV	5	2.3		σ_{fiss}	6.07–2.23 MeV	5	4.4	C	σ_{el}	2.23–1.35 MeV	5	3.4
		9.12–2.03 keV	3	2.1			2.23–1.35 MeV	5	4.5			1.35 MeV–498 keV	5	2.5
		2.03 keV–454 eV	3	2.7			1.35 MeV–498 keV	5	3.3			498–183 keV	5	3.3
	σ_{fiss}	6.07–2.23 MeV	5	2.2	Pu-241	σ_{fiss}	6.07–2.23 MeV	20	8.4	Si-28	σ_{capt}	19.6–6.07 MeV	20	8.1
		2.23–1.35 MeV	5	2.5			1.35 MeV–498 keV	10	5		σ_{inel}	6.07–2.23 MeV	30	4.4
	ν	6.07–2.23 MeV	2	1.7			498–183 keV	10	4.5			2.23–1.35 MeV	35	8.4
		2.23–1.35 MeV	2	1.9			183–67.4 keV	10	3.7					
	σ_{inel}	6.07–2.23 MeV	15	2.3			67.4–24.8 keV	10	3.7					
		2.23–1.35 MeV	10	2.6			24.8–9.12 keV	10	3.8					
		1.35 MeV–498 keV	10	3.6			9.12–2.03 keV	10	3.2					
Pu-238	σ_{fiss}	67.4–24.8 keV	30	9.9			2.03 keV–454 eV	10	4					
		24.8–9.12 keV	30	10.3	Pu-242	σ_{fiss}	1.35 MeV–498 keV	10	5.8					
		9.12–2.03 keV	30	8.7	Am-241	σ_{capt}	183–67.4 keV	10	5.1					
		2.03 keV–454 eV	30	10			67.4–24.8 keV	10	4.9					
Pu-239	σ_{capt}	183–67.4 keV	15	8.1			24.8–9.12 keV	10	5					
		24.8–9.12 keV	10	6			9.12–2.03 keV	10	4.2					
		9.12–2.03 keV	5	4.1			2.03 keV–454 eV	10	4.8					
		2.03 keV–454 eV	5	4.5		σ_{fiss}	6.07–2.23 MeV	10	4.7					
	σ_{fiss}	6.07–2.23 MeV	5	3.3			2.23–1.35 MeV	10	4.7					
		2.23–1.35 MeV	5	3.2			1.35 MeV–498 keV	10	4.4					
		1.35 MeV–498 keV	5	2	Cm-242	σ_{capt}	183–67.4 keV	40	26.8					
		498–183 keV	5	2			67.4–24.8 keV	40	26.7					
		183–67.4 keV	5	1.8			24.8–9.12 keV	40	26.5					
		67.4–24.8 keV	5	2			9.12–2.03 keV	40	21.7					
		24.8–9.12 keV	5	2.2			2.03 keV–454 eV	40	26.9					
		9.12–2.03 keV	5	1.9			454–22.6 eV	40	26.8					
		2.03 keV–454 eV	3	2.3										

Table 38
Results of the target accuracy study for the LFR reactor

Isotope	Cross-section	Energy range	Uncertainty		Isotope	Cross-section	Energy range	Uncertainty		Isotope	Cross-section	Energy range	Uncertainty	
			Initial	Required				Initial	Required				Initial	Required
U-238	σ_{capt}	1.35 MeV–498 keV	5	2.9	Pu-240	σ_{capt}	1.35 MeV–498 keV	20	8.4	Zr-90	σ_{el}	498–183 keV	20	9.8
		498–183 keV	5	2.4			498–183 keV	20	5.8			183–67.4 keV	20	10.8
		183–67.4 keV	5	2.4			183–67.4 keV	20	5.4			67.4–24.8 keV	20	10.3
		67.4–24.8 keV	5	2.4			67.4–24.8 keV	20	5.7		σ_{inel}	6.07–2.23 MeV	20	8.6
		24.8–9.12 keV	5	2.7			24.8–9.12 keV	10	6.8	Pb-206	σ_{capt}	183–67.4 keV	20	9.8
	σ_{fiss}	6.07–2.23 MeV	5	2.6		σ_{fiss}	6.07–2.23 MeV	5	4.1		σ_{el}	1.35 MeV–498 keV	20	6.3
		2.23–1.35 MeV	5	2.6			2.23–1.35 MeV	5	3.7			498–183 keV	20	7
	σ_{inel}	6.07–2.23 MeV	15	3.8			1.35 MeV–498 keV	5	2.1		σ_{inel}	19.6–6.07 MeV	40	15.9
		2.23–1.35 MeV	10	3.1			498–183 keV	5	4.1			6.07–2.23 MeV	40	4.6
		1.35 MeV–498 keV	10	2.9		ν	1.35 MeV–498 keV	2	1.8			2.23–1.35 MeV	40	4.4
		498–183 keV	10	4.2	Pu-241	σ_{fiss}	1.35 MeV–498 keV	10	4.9			1.35 MeV–498 keV	45	5.3
		183–67.4 keV	10	4.8			498–183 keV	10	3.5	Pb-207	σ_{el}	1.35 MeV–498 keV	20	6.8
Pu-238	σ_{fiss}	1.35 MeV–498 keV	10	4.5			183–67.4 keV	10	3.5			498–183 keV	20	7.5
		498–183 keV	10	4.5			67.4–24.8 keV	10	4.2		σ_{inel}	19.6–6.07 MeV	40	26.6
		183–67.4 keV	10	6.2			24.8–9.12 keV	10	4.9			6.07–2.23 MeV	40	5.5
		67.4–24.8 keV	30	7.4			9.12–2.03 keV	10	7.3			2.23–1.35 MeV	40	6.7
		24.8–9.12 keV	30	8.7	Pu-242	σ_{fiss}	1.35 MeV–498 keV	10	5.3			1.35 MeV–498 keV	45	4
		9.12–2.03 keV	30	12.8	Am-241	σ_{capt}	498–183 keV	10	7.3	Pb-208	σ_{el}	6.07–2.23 MeV	20	8.4
Pu-239	σ_{capt}	498–183 keV	15	5.7			183–67.4 keV	10	7.1			2.23–1.35 MeV	20	7.7
		183–67.4 keV	15	5.4		σ_{fiss}	1.35 MeV–498 keV	10	7.1			1.35 MeV–498 keV	20	3.7
		67.4–24.8 keV	10	6	Am-242m	σ_{fiss}	498–183 keV	20	10.9			498–183 keV	20	4.7
		24.8–9.12 keV	10	6.1	Cm-244	σ_{fiss}	1.35 MeV–498 keV	40	8.6		σ_{inel}	19.6–6.07 MeV	40	9.4
	σ_{fiss}	6.07–2.23 MeV	5	3.3	Cm-245	σ_{fiss}	1.35 MeV–498 keV	40	13.8			6.07–2.23 MeV	40	4.9
		2.23–1.35 MeV	5	2.9			498–183 keV	40	9.6		$\sigma_{n,2n}$	19.6–6.07 MeV	100	53.1
		1.35 MeV–498 keV	5	1.4			183–67.4 keV	40	10	B-10	σ_{capt}	1.35 MeV–498 keV	15	6.1
		498–183 keV	5	1.1			67.4–24.8 keV	40	11.5			498–183 keV	15	3.3
		183–67.4 keV	5	1.2			24.8–9.12 keV	40	14.1			183–67.4 keV	10	3
		67.4–24.8 keV	5	1.5	Fe-56	σ_{el}	183–67.4 keV	10	7.1			67.4–24.8 keV	10	3.7
		24.8–9.12 keV	5	1.9		σ_{inel}	6.07–2.23 MeV	15	8.5			24.8–9.12 keV	8	4.3
		9.12–2.03 keV	5	3			2.23–1.35 MeV	10	5.6			9.12–2.03 keV	8	6.7
	ν	498–183 keV	1	0.9			1.35 MeV–498 keV	20	4.8					

Table 39
Results of the target accuracy study for the SFR reactor

Isotope	Cross-section	Energy range	Uncertainty		Isotope	Cross-section	Energy range	Uncertainty		Isotope	Cross-section	Energy range	Uncertainty	
			Initial	Required				Initial	Required				Initial	Required
U-238	σ_{inel}	6.07–2.23 MeV	15	7.3	Pu-241	σ_{fiss}	6.07–2.23 MeV	20	8.8	Cm-245	σ_{fiss}	2.23–1.35 MeV	40	20.7
		2.23–1.35 MeV	10	6.8			2.23–1.35 MeV	10	7.8			1.35 MeV–498 keV	40	12
		1.35 MeV–498 keV	10	7.5			1.35 MeV–498 keV	10	4.6			498–183 keV	40	9
Np-237	σ_{fiss}	1.35 MeV–498 keV	10	8.3			498–183 keV	10	3.6			183–67.4 keV	40	9.1
Pu-238	σ_{fiss}	6.07–2.23 MeV	10	8			183–67.4 keV	10	3.5			67.4–24.8 keV	40	12
		2.23–1.35 MeV	10	7.6			67.4–24.8 keV	10	4.5			24.8–9.12 keV	40	12.2
		1.35 MeV–498 keV	10	4.5			24.8–9.12 keV	10	4.7			9.12–2.03 keV	40	19.5
		498–183 keV	10	4.9			9.12–2.03 keV	10	7.3			2.03 keV–454 eV	40	14.5
		183–67.4 keV	10	6.7			2.03 keV–454 eV	10	6	Fe-56	σ_{capt}	19.6–6.07 MeV	45	21.5
		67.4–24.8 keV	30	8.7	Pu-242	σ_{fiss}	6.07–2.23 MeV	10	7.1			183–67.4 keV	8	7.9
		24.8–9.12 keV	30	9.2			2.23–1.35 MeV	10	6.6			2.03 keV–454 eV	8	7.2
		9.12–2.03 keV	30	13.5			1.35 MeV–498 keV	10	4.8		σ_{el}	6.07–2.23 MeV	20	7.1
		2.03 keV–454 eV	30	10.6			498–183 keV	20	11.9			2.23–1.35 MeV	10	6.8
Pu-239	σ_{capt}	498–183 keV	15	9.4	Am-241	σ_{capt}	498–183 keV	10	9.2			1.35 MeV–498 keV	10	5
		183–67.4 keV	15	8.1			183–67.4 keV	10	8.3			498–183 keV	10	3.6
		67.4–24.8 keV	10	9		σ_{fiss}	6.07–2.23 MeV	10	9.3			183–67.4 keV	10	4.7
		24.8–9.12 keV	10	7.7			2.23–1.35 MeV	10	8.7		σ_{inel}	19.6–6.07 MeV	20	12.2
	σ_{fiss}	6.07–2.23 MeV	5	3.9			1.35 MeV–498 keV	10	7.9			6.07–2.23 MeV	15	5.6
		2.23–1.35 MeV	5	3.6	Am-242m	σ_{capt}	498–183 keV	40	19.8			2.23–1.35 MeV	10	4.5
		1.35 MeV–498 keV	5	2.1			183–67.4 keV	40	15.7			1.35 MeV–498 keV	20	4.3
		498–183 keV	5	1.8		σ_{fiss}	6.07–2.23 MeV	20	11.1	Cr-52	σ_{el}	1.35 MeV–498 keV	10	9.5
		183–67.4 keV	5	2			2.23–1.35 MeV	20	11.3			498–183 keV	10	8.1
		67.4–24.8 keV	5	2.8			1.35 MeV–498 keV	20	5.8			183–67.4 keV	10	8.6
		24.8–9.12 keV	5	3.1			498–183 keV	20	4.2		$\sigma_{n,2n}$	19.6–6.07 MeV	100	17.1
Pu-240	σ_{capt}	1.35 MeV–498 keV	20	10.2			183–67.4 keV	20	4.2	Zr-90	σ_{el}	498–183 keV	20	14.1
		498–183 keV	20	7.3			67.4–24.8 keV	20	5.5		σ_{inel}	6.07–2.23 MeV	20	12
		183–67.4 keV	20	6.1			24.8–9.12 keV	10	5.7	Na-23	σ_{inel}	6.07–2.23 MeV	30	11.7
		67.4–24.8 keV	20	6.6			9.12–2.03 keV	10	8.8			2.23–1.35 MeV	30	12.5
		24.8–9.12 keV	10	6.7			2.03 keV–454 eV	10	7			1.35 MeV–498 keV	30	5.4
		2.03 keV–454 eV	10	7.6	Am-243	σ_{capt}	183–67.4 keV	10	9.7	B-10	σ_{capt}	1.35 MeV–498 keV	15	12.5
	σ_{fiss}	6.07–2.23 MeV	5	3.7		σ_{fiss}	1.35 MeV–498 keV	10	9.8			498–183 keV	15	7
		2.23–1.35 MeV	5	3.6	Cm-244	σ_{capt}	183–67.4 keV	40	20.3			183–67.4 keV	10	5.9
		1.35 MeV–498 keV	5	2.5		σ_{fiss}	6.07–2.23 MeV	40	11.3			67.4–24.8 keV	10	6.9
							2.23–1.35 MeV	40	11.3			24.8–9.12 keV	8	7.7
							1.35 MeV–498 keV	40	7					
							498–183 keV	40	16.4					

Table 40
Results of the target accuracy study for the EFR reactor

Isotope	Cross-section	Energy range	Uncertainty		Isotope	Cross-section	Energy range	Uncertainty		Isotope	Cross-section	Energy range	Uncertainty	
			Initial	Required				Initial	Required				Initial	Required
U-238	σ_{capt}	1.35 MeV–498 keV	5	3.7	Pu-240	σ_{capt}	1.35 MeV–498 keV	20	11	Cm-243	σ_{fiss}	6.07–2.23 MeV	40	28.9
		498–183 keV	5	3.2			498–183 keV	20	7.4			2.23–1.35 MeV	40	29.2
		183–67.4 keV	5	2.6			183–67.4 keV	20	5.4			1.35 MeV–498 keV	40	14
		67.4–24.8 keV	5	2.2			67.4–24.8 keV	20	4.9			498–183 keV	40	12.1
		24.8–9.12 keV	5	2.1			24.8–9.12 keV	10	5.1			183–67.4 keV	40	10.6
		9.12–2.03 keV	3	2.5			9.12–2.03 keV	10	6.2			67.4–24.8 keV	40	11.9
		2.03 keV–454 eV	3	2.4			2.03 keV–454 eV	10	4.7			24.8–9.12 keV	40	13
	σ_{fiss}	6.07–2.23 MeV	5	3.1		σ_{fiss}	6.07–2.23 MeV	5	4.9			9.12–2.03 keV	40	14.3
		2.23–1.35 MeV	5	3.6			1.35 MeV–498 keV	5	3.5			2.03 keV–454 eV	40	12.9
	σ_{inel}	6.07–2.23 MeV	15	4	Pu-241	σ_{capt}	24.8 keV–9.12 keV	20	14.5	Cm-244	σ_{capt}	1.35 MeV–498 keV	40	26.8
		2.23–1.35 MeV	10	4.3			9.12–2.03 keV	20	15.3			498–183 keV	40	17.2
		1.35 MeV–498 keV	10	5.3			2.03 keV–454 eV	20	13			183–67.4 keV	40	13.2
	$\sigma_{n,2n}$	19.6–6.07 MeV	30	10.9		σ_{fiss}	6.07–2.23 MeV	20	10.6			67.4–24.8 keV	40	11.5
Pu-238	σ_{capt}	2.03 keV–454 eV	20	18.9			2.23–1.35 MeV	10	9.9			24.8–9.12 keV	40	11.8
	σ_{fiss}	67.4–24.8 keV	30	16.6			1.35 MeV–498 keV	10	5.7			9.12–2.03 keV	40	22.8
		24.8–9.12 keV	30	17.8			498–183 keV	10	4.5			2.03 keV–454 eV	40	15.1
		9.12–2.03 keV	30	19.9			183–67.4 keV	10	3.8			454–22.6 eV	40	23.9
		2.03 keV–454 eV	30	15.8			67.4–24.8 keV	10	4.1		σ_{fiss}	6.07–2.23 MeV	40	19.6
Pu-239	σ_{capt}	1.35 MeV–498 keV	15	12			24.8–9.12 keV	10	4.3			2.23–1.35 MeV	40	21.3
		498–183 keV	15	7.1			9.12–2.03 keV	10	4.8			1.35 MeV–498 keV	40	13.2
		183–67.4 keV	15	5.3			2.03 keV–454 eV	10	4.3			498–183 keV	40	30.7
		67.4–24.8 keV	10	5	Am-241	σ_{capt}	183–67.4 keV	10	9.8	Cm-245	σ_{capt}	183–67.4 keV	40	30.4
		24.8–9.12 keV	10	4.4	Am-242m	σ_{capt}	183–67.4 keV	40	32.7			67.4–24.8 keV	40	30.9
		9.12–2.03 keV	5	4.1		σ_{fiss}	183–67.4 keV	20	19.4			2.03 keV–454 eV	40	31.5
		2.03 keV–454 eV	5	3.4			67.4–24.8 keV	20	19.2		σ_{fiss}	6.07–2.23 MeV	40	30.2
	σ_{fiss}	6.07–2.23 MeV	5	3.4	Cm-242	σ_{capt}	498–183 keV	40	18.6			2.23–1.35 MeV	40	29.7
		2.23–1.35 MeV	5	3.4			183–67.4 keV	40	12.9			1.35 MeV–498 keV	40	17.4
		1.35 MeV–498 keV	5	1.9			67.4–24.8 keV	40	10.4			498–183 keV	40	14.3
		498–183 keV	5	1.8			24.8–9.12 keV	40	10			183–67.4 keV	40	12.5
		183–67.4 keV	5	1.7			9.12–2.03 keV	40	11.4			67.4–24.8 keV	40	13.5
		67.4–24.8 keV	5	2			2.03 keV–454 eV	40	9.2			24.8–9.12 keV	40	14.6
		24.8–9.12 keV	5	2.3			454–22.6 eV	40	18			9.12–2.03 keV	40	16.6
		9.12–2.03 keV	5	2.7		σ_{fiss}	6.07–2.23 MeV	40	28.9			2.03 keV–454 eV	40	14.5
		2.03 keV–454 eV	3	2.2			2.23–1.35 MeV	40	29.1			454–22.6 eV	40	30.9
	$\sigma_{n,2n}$	19.6–6.07 MeV	50	32.4			1.35 MeV–498 keV	40	18.4	Fe-56	σ_{inel}	6.07–2.23 MeV	15	6.7
Na-23	σ_{inel}	6.07–2.23 MeV	30	13.1			498–183 keV	40	29.3			2.23–1.35 MeV	10	7.2
		1.35 MeV–498 keV	30	8.7	O-16	σ_{capt}	6.07–2.23 MeV	20	11.7			1.35 MeV–498 keV	20	9.1
						σ_{el}	498–183 keV	5	4.9	Cr-52	$\sigma_{n,2n}$	19.6–6.07 MeV	100	22.3

Table 41
Results of the target accuracy study for the VHTR reactor

Isotope	Cross-section	Energy range	Uncertainty		Isotope	Cross-section	Energy range	Uncertainty	
			Initial	Required				Initial	Required
U-236	σ_{capt}	22.6–4.00 eV	8	7.1	Pu-241	σ_{fiss}	454–22.6 eV	10	8.1
U-238	σ_{capt}	454–22.6 eV	3	1.9			22.6–4.00 eV	10	5.5
		22.6–4.00 eV	3	1.4			0.54–0.10 eV	2	1.9
Pu-239	σ_{capt}	0.54–0.10 eV	3	1.1	Am-241	σ_{capt}	0.54–0.10 eV	10	9.4
	σ_{fiss}	0.54–0.10 eV	2	1	Am-243	σ_{capt}	4.00–0.54 eV	20	12.4
Pu-240	σ_{capt}	454–22.6 eV	10	9.6	C	σ_{scatt}	6.07–2.23 MeV	35	12.3
		4.00–0.54 eV	7	1.1					

8. Optimized integral experiments

In order to plan for specific experiments able to reduce uncertainties on selected design parameters, a formal approach, initially proposed by Usachev et al. (1973) has been applied by Palmiotti and Salvatores (1984) and further developed by Gandini (1988).

In the case of a reference parameter R, once the sensitivity coefficient matrix S_R and the covariance matrix D are available, the uncertainty on the integral parameter can be evaluated, as shown in Section 2.1, by the equation:

$$\Delta R_0^2 = S_R^+ D S_R. \tag{20}$$

We can consider an integral experiment conceived in order to reduce the uncertainty ΔR_0^2. Let us indicate by S_E the sensitivity matrix associated with this experiment. If we call "representativity factor" the following expression:

$$r_{RE} = \frac{(S_R^+ D S_E)}{[(S_R^+ D S_R)(S_E^+ D S_E)]^{1/2}}, \tag{21}$$

it can be shown (Usachev et al., 1973) that the uncertainty on the reference parameter R is reduced by:

$$\Delta R_0'^2 = \Delta R_0^2 \cdot (1 - r_{RE}^2). \tag{22}$$

From this expression it is clear that the experiment should be conceived in such a way that the sensitivity matrices S_E and S_R are as similar as possible, i.e. r_{RE}^2 should be as close to 1 as possible.

If more than one experiment is available, the Eq. (22) can be generalized. In the case of two experiments, characterized by sensitivity matrices S_{E1} and S_{E2} the following expression (Gandini, 1988) can be derived:

$$\begin{aligned}\Delta R_0'^2 &= S_R^+ D' S_R \\ &= \Delta R_0^2 \left[1 - \frac{1}{1 - r_{12}^2}(r_{R1} - r_{R2})^2 - \frac{2}{1 + r_{12}} r_{R1} r_{R2}\right],\end{aligned} \tag{23}$$

where D' is the new covariance matrix and

$$r_{12} = \frac{(S_{E1}^+ D S_{E2})}{[(S_{E1}^+ D S_{E1})(S_{E2}^+ D S_{E2})]^{1/2}} \tag{24}$$

$$r_{R1} = \frac{(S_R^+ D S_{E1})}{[(S_R^+ D S_R)(S_{E1}^+ D S_{E1})]^{1/2}} \tag{25}$$

$$r_{R2} = \frac{(S_R^+ D S_{E2})}{[(S_R^+ D S_R)(S_{E2}^+ D S_{E2})]^{1/2}}. \tag{26}$$

From Eq. (23) it is clear that the two experiments should bring complementary information, i.e., r_{12} should be as different as possible from 1.

The approach outlined here can be used to plan optimized integral experiments to reduce uncertainties on a set of integral parameters of a reference system.

9. Conclusions

Sensitivity and uncertainty analysis have been performed for reactor systems that have been considered under the US Department of Energy Gen IV and AFCI programs. The results obtained on a wide range of integral parameters show that the impact of assumed cross-section data uncertainties is in some cases significant. However, no crucial issue is found that would prevent the use of the data for feasibility or pre-conceptual design studies. This conclusion is obviously dependent on the assumed uncertainty data and the type of system considered. Better and more consistent covariance data would consolidate this conclusion.

Moreover, to propose a credible program of new cross-section measurements, it is necessary to show the impact of the existing data uncertainties on relevant parameters, taking into account design parameters target accuracies. For this purpose, we have also considered a preliminary set of design target accuracies which could be relevant in subsequent design phases and we have evaluated nuclear data improvement requirements. In some cases, very stringent requirements have been obtained that will be difficult to achieve even with very sophisticated measurement techniques or/and evaluations. These requirements indicated that a careful analysis is needed in order to define the most appropriate and effective strategy for data uncertainty reduction.

In this respect, it is stressed that integral experiments and statistical data adjustments are currently powerful tools to overcome most difficulties, since they provide a global validation of data, and guidance for developing improved evaluations for selected isotopes, reaction types and energy domains.

However a statistical data adjustments strategy should satisfy a number of conditions:

Table 42
Results of the target accuracy study for the PWR reactor

Isotope	Cross-section	Energy range	Uncertainty		Isotope	Cross-section	Energy range	Uncertainty		Isotope	Cross-section	Energy range	Uncertainty	
			Initial	Required				Initial	Required				Initial	Required
U-235	σ_{capt}	454–22.6 eV	5	2.4	Pu-240	σ_{capt}	454–22.6 eV	10	4	Cm-243	σ_{capt}	454–22.6 eV	40	26.1
		22.6–4.00 eV	5	2.5			4.00–0.54 eV	7	0.6			22.6–4.00 eV	40	25.7
U-238	σ_{capt}	67.4–24.8 keV	5	3.9			0.54–0.10 eV	3	2.3			4.00–0.54 eV	40	17.7
		24.8–9.12 keV	5	3.3	Pu-241	σ_{capt}	0.54–0.10 eV	3	2.2			0.54–0.10 eV	40	25.7
		9.12–2.03 keV	3	2.4			0.10 eV-thermal	3	2.7			0.10 eV-thermal	40	25.3
		2.03 keV–454 eV	3	1.9		σ_{fiss}	454–22.6 eV	10	3.5		σ_{fiss}	454–22.6 eV	40	18.9
		454–22.6 eV	3	1			22.6–4.00 eV	10	2.5			22.6–4.00 eV	40	12.9
		22.6–4.00 eV	3	1			0.54–0.10 eV	2	1.3			4.00–0.54 eV	40	7.5
	σ_{fiss}	6.07–2.23 MeV	5	1.8			0.10 eV-thermal	2	1.4			0.54–0.10 eV	40	13.5
		2.23–1.35 MeV	5	2.4	Pu-242	σ_{capt}	4.00–0.54 eV	5	2.4			0.10 eV-thermal	40	14.4
	ν	6.07–2.23 MeV	2	1.6	Am-241	σ_{capt}	0.54–0.10 eV	10	5.6	Cm-244	σ_{capt}	2.03 keV–454 eV	40	25.7
	σ_{scatt}	6.07–2.23 MeV	15	3.8	Am-242m	σ_{capt}	4.00–0.54 eV	40	26.3			454–22.6 eV	40	14.4
	$\sigma_{n,2n}$	19.6–6.07 MeV	30	7.9			0.54–0.10 eV	40	25.3			22.6–4.00 eV	40	4.1
Np-237	σ_{capt}	454–22.6 eV	10	6.1			0.10 eV-thermal	40	26.3			0.54–0.10 eV	40	25.7
		4.00–0.54 eV	10	4.7	Am-243	σ_{capt}	454–22.6 eV	20	17.7			0.10 eV-thermal	40	25.7
		0.54–0.10 eV	4	3.4			22.6–4.00 eV	20	15.4	Cm-245	σ_{capt}	4.00–0.54 eV	40	26
Pu-238	σ_{capt}	0.54–0.10 eV	10	5.5			4.00–0.54 eV	20	3.4			0.54–0.10 eV	40	24.6
		0.10 eV-thermal	10	3.5			0.54–0.10 eV	20	19.9			0.10 eV-thermal	40	17.6
	σ_{fiss}	454–22.6 eV	30	22.7	Cm-242	σ_{capt}	67.4–24.8 keV	40	26.1		σ_{fiss}	454–22.6 eV	40	22.8
Pu-239	σ_{capt}	454–22.6 eV	5	3			24.8–9.12 keV	40	25.9			22.6–4.00 eV	40	16.8
		22.6–4.00 eV	5	3.1			9.12–2.03 keV	40	19.6			4.00–0.54 eV	40	15.9
		0.54–0.10 eV	3	0.7			2.03 keV–454 eV	40	15.3			0.54–0.10 eV	40	8.4
		0.10 eV-thermal	2	1.5			454–22.6 eV	40	5.6			0.10 eV-thermal	40	6.1
	σ_{fiss}	454–22.6 eV	3	2.5			22.6–4.00 eV	40	7.8	O	σ_{capt}	6.07–2.23 MeV	20	7.4
		22.6–4.00 eV	3	2.3			4.00–0.54 eV	40	25.7	H	σ_{scatt}	4.00–0.54 eV	1	0.8
		0.54–0.10 eV	2	0.6			0.54–0.10 eV	40	15.8	Zr	σ_{scatt}	6.07–2.23 MeV	20	6
		0.10 eV-thermal	1	0.9			0.10 eV-thermal	40	14.5					

Table 43
GFR, LFR, SFR, and EFR uncertainties (%)

Reactor	K_{eff}	Power peak	Temperature reactivity coefficient	Void reactivity coefficient	Burnup $\Delta\rho$	Decay heat	Dose	Neutron source
GFR Initial[a]	±1.20	±1.18	±3.56	±4.83	±22.18	±0.32	±0.39	±1.15
GFR final[b]	0.57	0.76	2.17	3.51	14.05	0.20	0.23	1.07
LFR initial	1.51	0.75	5.24	12.99	12.12	0.31	0.36	0.80
LFR final	0.53	0.31	3.32	2.80	4.79	0.16	0.32	0.62
SFR initial	1.10	0.36	4.09	17.75	3.92	0.24	0.16	0.60
SFR final	0.53	0.24	2.78	6.86	1.77	0.10	0.08	0.32
EFR initial	1.02	0.70	3.39	8.40	7.14	1.59	1.10	3.87
EFR final	0.53	0.48	2.14	4.57	3.52	0.85	0.61	2.10

[a] With data uncertainty values by Palmiotti and Salvatores (2005).
[b] With target accuracy requirement.

Table 44
VHTR uncertainties (%)

	K_{eff}		Peak		Temperature reactivity coefficient		Burnup $\Delta\rho$	Decay heat	Dose	Neutron source
	BOC	EOC	BOC	EOC	BOC	EOC				
Initial[a]	±0.41	±0.94	±0.87	±0.93	±3.62	±5.76	±5.74	±2.49	±1.92	±12.19
Final[b]	0.32	0.43	0.52	0.52	3.19	2.77	1.95	1.35	1.19	8.27

[a] With data uncertainty values by Palmiotti and Salvatores (2005).
[b] With target accuracy requirement.

Table 45
PWR uncertainties (%)

	K_{eff}		Temperature reactivity coefficient		Burnup $\Delta\rho$	Decay heat	Dose	Neutron source
	BOC	EOC	BOC	EOC				
Initial[a]	±0.33	±0.97	±2.07	±4.01	±4.00	±2.89	±2.34	±11.23
Final[b]	0.23	0.43	1.24	1.65	1.09	1.28	1.05	2.90

[a] With data uncertainty values by Palmiotti and Salvatores (2005).
[b] With target accuracy requirement.

Table 46
Uncertainty on nuclide density n_{t_F} (%) at end of cycle

	U^{235}	U^{238}	Np^{237}	Pu^{238}	Pu^{239}	Pu^{240}	Pu^{241}	Pu^{242}	Am^{241}	Am^{242m}	Am^{243}	Cm^{242}	Cm^{243}	Cm^{244}	Cm^{245}	Cm^{246}
GFR initial[a]	±0.2	±0.0	±0.6	±0.9	±0.3	±0.3	±0.9	±0.3	±0.5	±3.1	±0.6	±3.5	±8.3	±1.2	±3.2	±3.5
GFR final[b]	0.2	0.0	0.6	0.6	0.2	0.2	0.5	0.2	0.3	1.7	0.6	1.9	5.3	1.2	3.2	3.5
LFR initial	0.4	0.0	0.4	0.5	0.3	0.2	1.4	0.2	0.4	1.5	0.5	3.7	4.7	0.9	2.8	0.7
LFR final	0.4	0.0	0.4	0.3	0.1	0.1	0.5	0.1	0.3	1.3	0.5	3.1	4.7	0.7	1.7	0.7
SFR initial	0.4	0.0	0.2	0.3	0.2	0.1	0.6	0.1	0.3	0.9	0.3	2.0	2.5	0.7	1.8	0.6
SFR final	0.4	0.0	0.2	0.2	0.1	0.1	0.3	0.1	0.2	0.3	0.3	1.9	2.5	0.4	1.0	0.6
EFR initial	2.8	0.2	12.9	3.1	1.4	1.4	4.8	1.7	2.9	5.3	3.0	2.1	16.4	4.5	13.9	5.5
EFR final	2.8	0.1	5.1	2.4	0.7	0.7	1.9	1.4	2.7	5.1	3.0	1.7	5.3	2.4	5.2	5.0
VHTR initial	0.7	0.1	5.5	5.4	2.2	6.2	3.0	4.0	5.9	6.9	6.8	4.5	21.5	13.1	34.5	
VHTR final	0.7	0.1	5.0	5.0	1.1	1.5	1.6	2.6	4.9	6.2	5.1	3.1	21.2	9.0	33.0	
PWR initial	1.3	0.1	5.7	5.6	1.8	6.0	2.7	3.8	5.9	6.3	9.2	3.1	25.1	11.9	32.7	
PWR final	1.2	0.0	2.8	2.7	0.6	0.9	1.0	1.8	3.9	4.2	2.7	1.2	5.1	3.0	5.1	

[a] With data uncertainty values by Palmiotti and Salvatores (2005).
[b] With target accuracy requirement.

- The integral experiments used in the adjustment procedure should be "clean" and "representative", in the sense that the associated experimental uncertainties are small and well understood and should be defined according to criteria and procedures of the type outlined in this paper (see Section 8).

- The calculated values for integral experiments should not be affected by any significant modeling uncertainty (e.g., geometrical description, number of energy group used in the analysis, etc.), in order to avoid the introduction of systematic errors and biases.
- As aforementioned, the covariance data should be reliable, complete, and consistent.
- Data adjustments should as much as possible relate to the physics parameters which describe the cross-sections, to make adjustments independent from the energy collapsing procedures.

In summary, it is important to stress once more that better uncertainty data will play an essential role both in assessing needs for new data with reduced uncertainties and in design oriented statistical data adjustments.

As far as design target accuracies are concerned, it is expected that the evolution of the Gen IV system analysis, and the focusing on a few preferred concepts, will motivate designers to define fully justified target accuracies, based on safety and economics criteria. Nevertheless, the present study contributes to setting general guidelines that can be used in the physics assessment of future systems.

Acknowledgement

Part of this work was supported by the US Department of Energy, Nuclear Energy Programs, under Contract W-31-109-ENG-38.

References

Aliberti, G., Palmiotti, G., Salvatores, M., Stenberg, C.G., 2004. Transmutation dedicated systems: An assessment of nuclear data uncertainty impact. Nucl. Sci. Eng. 146, 13–50.

Bell, J., 1973. ORIGEN – The ORNL Isotope Generation and Depletion Code. Oak Ridge National Laboratory.

Cecchini, G., Farinelli, U., Gandini, A., Salvatores, M., 1964. Analysis of integral data for few group parameter evaluation of fast reactors. A/CONF 28/P/627, Geneva, Switzerland.

Courcelle, A. et al., 2004. JEF2.2 Nuclear data statistical adjustment using post-irradiation experiments. In: Proceedings of International Conference on PHYSOR-2004, 25–29 April, Chicago, IL, USA.

Forsberg, C.W., 2005. Brayton power cycles and high-temperature salt-cooled reactors. Trans. Am. Nucl. Soc. 92, 231.

Gandini, A., 1967. J. Nucl. Energy 21, 755.

Gandini, A., 1988. In: Ronen, Y. (Ed.), Uncertainty analysis and experimental data transposition methods in uncertainty analysis. CRC Press, Boca Raton.

Gandini, A., Palmiotti, G., Salvatores, M., 1986. Equivalent generalized perturbation theory (EGPT). Ann. Nucl. Energy 13, 109.

Gill, P.E., Murray, W., Saunders, M.A., 1997. SNOPT: An SQP algorithm for large-scale constrained programming. Technical Report SOL 97-3, Systems Optimization Laboratory, Department of Operations Research, Stanford University, Stanford, CA 94305-4022.

Gruppelaar, H.,1998. Status of pseudo-fission product cross-sections for fast reactors. Report by the WP on Int. Eval. Co-operation of the NEA Nucl. Sci. Committee and NEA and NEA/WPEC-17.

Kallfelz, J.M., Bruna, G., Palmiotti, G., Salvatores, M., 1977. Burn-up calculations with time-dependent generalized perturbation theory. Nucl. Sci. Eng. 62, 304.

Kawai, M., 2002. Evaluation method of inelastic scattering cross-section for weakly absorbing fission product nuclides. Report by the WP on Int. Eval. Co-operation of the NEA Nucl. Sc. Committee and NEA and NEA/WPEC-10.

Kim, T.K., Taiwo, T.A., Yang, W.S., Palmiotti, G., 2005. Sensitivity study of design parameters for liquid-salt-cooled VHTR. Trans. Am. Nucl. Soc., 93.

Kodeli, I., Sartori, E., ZZ-COV-15GROUP-2005, NEA-1730 Package. OECD/NEA Data Bank (in preparation).

Koning, A., 2004. Code TALYS Monte-Carlo and covariances. Annual Mtg of the CSEWG, National Nuclear Data Center, Brookhaven National Laboratory.

Lubitz, C.R., 2004. Epithermal capture cross-sections of U-235. Report by the WP on Int. Eval. Co-operation of the NEA Nucl. Sc. Committee, NEA/WPEC-18.

Marcian, R. et al., 2004. Assessment of CASMO-4 prediction of the isotopic inventory of high burn-up MOX fuel. In: Proceedings of International Conference PHYSOR-2004, 25–29 April, Chicago, IL, USA.

Obložinský, P., 2005. Assessment of neutron cross-sections evaluations for the bulk of fission products. Report by the WP on Int. Eval. Co-operation of the NEA Nucl. Sci. Committee, ISBN-92-64-01063-7 and NEA/WPEC-21.

OECD/NEA Data Bank, 2005. The JEFF-3.0 Nuclear Data Library. JEFF Report 19.

Palmiotti, G., Salvatores, M., 1984. Use of integral experiments in the assessment of large liquid-metal fast breeder reactor basic design parameters. Nucl. Sci. Eng. 87, 333.

Palmiotti, G., Salvatores, M., 1988. Multidimensional transport sensitivity for shielding analysis. In: Seventh International Conference on Reactor Shielding, Bournemouth, UK.

Palmiotti, G., Salvatores, M., 2005. Proposal for nuclear data covariance matrix. JEFDOC 1063 Rev. 1.

Palmiotti, G., Rieunier, J.M., Gho, C., Salvatores, M., 1990. BISTRO optimized two dimensional Sn transport code. Nucl. Sci. Eng. 104, 26.

Palmiotti, G., Salvatores, M., Hill, R.N., 1994. Sensitivity, uncertainty assessment, and target accuracies related to radiotoxicity evaluation. Nucl. Sci. Eng. 117, 239.

Palmiotti, G., Aliberti, G., Salvatores, M., Tommasi, J., 2004. Integral experiment analysis for validation and improvement of minor actinide data for transmutation needs. In: Proceedings of International Conference on ND-2004, September, Santa Fe, NM, USA.

Rimpault, G. et al., 2002. The ERANOS code and data system for fast reactor neutronic analyses, In: Proceedings of PHYSOR 2002 Conference, Seoul, Korea.

Santamarina, A., 2005. Private communication. See also JEFDOC 1008, 2004.

Smith, D.L., 2004. Covariance matrices for nuclear cross-sections derived from nuclear model calculations. Report ANL/NDM-159, Argonne National Laboratory.

Smith, D.L., 2005. Neutron reaction data for IFMIF: pointing the way forward. In: IAEA Technical Mtg "Nuclear Data for IFMIF", 4–6 October, Karlsruhe, Germany.

Tommasi, J., Dupont, E., Marimbeau, P. Analysis of sample irradiation experiments in Phénix for JEFF-3.0 nuclear data validation. Nucl. Sci. Eng. (in press).

Trakas, C., Dandin, L., 2004. Benchmarking of MONTEBURNS against measurements on irradiated UOX and MOX fuels. In: Proceedings of International Conference PHYSOR-2004, 25–29 April, Chicago, IL, USA.

Usachev, L.M. et. al., 1973. IAEA Publication, Conference 730302, vol. 1, p. 129.

US Department of Energy Office of Nuclear Energy, Science, and Technology, 2005. Advanced Fuel Cycle Initiative: Objectives, Approach, and Technology Summary.

USDOE, 2002. Technology Roadmap for Generation IV Nuclear Energy Systems. GIF-002-00.